Ectopic expression of a mechanosensitive channel confers spatiotemporal resolution to ultrasound stimulations of neurons for visual restoration

Sara Cadoni, Charlie Demené, Ignacio Alcala, Matthieu Provansal, Diep Nguyen, Dasha Nelidova, Guillaume Labernède, Jules Lubetzki, Ruben Goulet, Emma Burban, et al.

Title:

Ectopic expression of a mechanosensitive channel confers spatiotemporal resolution to ultrasound stimulations of neurons for visual restoration

Author list:

Sara Cadoni[1], Charlie Demené[2], Ignacio Alcala[1], Matthieu Provansal[1], Diep Nguyen[1], Dasha Nelidova [3], Guillaume Labernede[1], Jules Lubetzki[1], Ruben Goulet[1], Emma Burban[1], Julie Dégardin[1], Manuel Simonutti[1], Gregory Gauvain[1], Fabrice Arcizet[1], Olivier Marre[1], Deniz Dalkara[1], Botond Roska[3], José Alain Sahel[1,4,5,6], Mickael Tanter[2*], Serge Picaud[1*]

Affiliation:

[1]Sorbonne Université, INSERM, CNRS, Institut de la Vision, 17 rue Moreau, F-75012 Paris, France;

[2]Physics for Medicine Paris, INSERM, CNRS, École Supérieure de Physique et de Chimie Industrielles (ESPCI Paris), Paris Sciences et Lettes (PSL) Research University, 75012 Paris, France;

[3]Institute of Molecular and Clinical Ophthalmology Basel, Basel, Switzerland;

[4]Department of Ophthalmology, The University of Pittsburgh School of Medicine, Pittsburgh, PA 15213, United States;

[5]Department of Ophthalmology and Vitreo-Retinal Diseases, Fondation Ophtalmologique Rothschild, F-75019 Paris, France;

[6]Centre Hospitalier National d'Ophtalmologie des XV-XX, F-75012 Paris.

[*]These authors contributed equally to this work.

Corresponding author: Serge Picaud (serge.picaud@inserm.fr)

http://www.researcherid.com/rid/H-4012-2014

Abstract

Remote and precisely controlled activation of the brain is a fundamental challenge in the development of brain-machine interfaces (BMI) for neurological treatments. Low-frequency ultrasound stimulation can be used to modulate neuronal activity deep in the brain especially after expressing ultrasound-sensitive proteins. But so far, no study has described an ultrasound-mediated activation strategy whose spatiotemporal resolution and acoustic intensity are compatible with the mandatory needs of BMIs, in particular for visual restoration. Here we combined the expression of large-conductance mechanosensitive ion channels (MscL) with uncustomary high-frequency ultrasonic stimulation to activate retinal or cortical neurons over millisecond durations at a spatiotemporal resolution and acoustic energy deposit compatible with vision restoration. The *in vivo* sonogenetic activation of the visual cortex generated a behaviour associated to light perception. Our findings demonstrate that sonogenetics can deliver millisecond pattern presentations via an approach less invasive than current BMIs for visual restoration.

Main text

Introduction

Brain-machine interfaces (BMIs) based on multi-electrode arrays have met with increasing success in peripheral sensory system rehabilitation strategies, for restoring hearing in the cochlea or sight in the retina[1, 2]. The restoration of vision is the most demanding challenge for BMIs, as it ultimately requires the 13Hz rate transmission of complex spatial patterns[3]. Although form perception can be achieved by epicortical or intracortical implants[4, 5], lack of long-term sustainability has intensified the search for non-contact distant activation of neuronal circuits. Optogenetic therapy has provided an alternative, as demonstrated on the retina even at the clinical level[6]. Despite encouraging animal studies[7-9], approaches for optical stimulation of the cortex are hindered by the dura mater and by brain scattering and absorption of light requiring invasive light guides[10].

Ultrasound (US) waves could potentially overcome these limitations to achieve the non-contact neuromodulation of cortical and subcortical areas of the brains[11-17]. However, this neuromodulation requires a craniotomy (Fig 1.a) and the use of high US frequencies to reach the required spatial resolution. Switching from 0.5 MHz to 15 MHz would theoretically lead to a 30-fold improvement in resolution (Fig. 1c-e) and a ~27000-fold improvement in neuromodulated volume. Unfortunately, most existing US neuromodulation strategies are restricted to low-frequency[15] or mid-range[18] transmissions resulting in poor spatial resolution (>3 mm) and/or long lasting responses while 30 MHz high frequency was reported to generate inhibitory neuromodulation[19]. Other attempts at high-frequency neuromodulation have resulted in high levels of acoustic energy[20], with risks of thermal heating[21] and tissue damage[14].

Sonogenetic therapy has proposed to generate a neuronal mechano-sensitivity by ectopic expression of US-sensitive proteins like TRP1 ion channel[22], mechanosensitive ion channel of large conductance (MscL)[23], or auditory-sensing protein prestin[24] using AAV gene delivery to target specific cell populations[23, 25, 26] nevertheless without spatiotemporal resolution compatible for vision restoration. A high temporal resolution was shown for MscL only in primary cultured hippocampal neurons with mutations enhancing its pressure sensitivity[27, 28],the MscL-G22S mutant boosting US sensitivity of *in vivo* neurons[23].

We have here investigated if we can use the MscL channel[29] 1) to boost the neuronal sensitivity to US not only *ex vivo* but also *in vivo* , 2) to target a locally defined subset of neurons by gene therapy, 3) to induce responses with a temporal precision (millisecond time delay and recovery) sufficient for visual restoration and 4) to gain more than one order of magnitude in spatial resolution through the *in vivo* use of high-frequency US at low acoustic intensities to prevent adverse effects[20].

Sonogenetic activation on the *ex vivo* retina

Using the retina as an easily accessible part of the central nervous system, we targeted MscL specifically into rat retinal ganglion cells (RGCs), with *in vivo* intravitreal delivery by an adeno-associated vector (AAV) encoding the *mscL* gene from *Escherichia coli* in its wild-type (WT) form or with the G22S mutation[28]. An AAV2.7m8[30] serotype vector was used to encode MscL fused to the red fluorescent protein tdTomato, under control of the SNCG promoter to target the RGC population[31]. On the eye fundus, tdTomato fluorescence was detected *in vivo* (Fig. 2a). Its expression was restricted to RGCs, as indicated by their double labeling with a specific RGC antibody, RPBMS (Figs 2b, E1b). Expression of the MscL channel seemed to be concentrated at the cell membrane on the soma and axon (Figs 2c, E1) with 24% and 46% of RPBMS-positive cells expressing tdTomato, for the MscL-WT and MscL-G22S proteins, respectively (Fig. 2d).

During *ex vivo* recordings of the MscL-expressing retina (Fig. 2e), RGCs displayed strong and sustained ON spiking responses to focused 15 MHz US stimulation (Fig. 2f- left) irrespectively of their ON or OFF responses to light (Fig. E2a). Many RGCs presented responses with very short latencies, 12.2±2.5 ms, (Fig. 2f- left), but some had longer latencies (Fig. 2g). By contrast, non-transfected (NT) retina displayed only long latency responses, 50.4 ± 4.2 ms (Figs 2f-right, 2g). Synaptic blockers (CNQX-LAP4-CPP) abolished US responses in non-transfected retinas but not in MscL-transfected retinas, in which they decreased the number of long latency US responses (LL: latency of more than 45 ms, Fig. 2l, Fig E2c-d). This observation suggests that responses in non-transfected retina originate upstream from RGCs, as previously reported[41]. This conclusion was supported by the absence of US response in the retinas of non-transfected blind P23H rats having lost photoreceptors whereas transfected P23H showed a majority of short latency (SL) responses (<45ms) (Fig. 2l, Fig E2c-d). The

geometric mean latencies in MscL-tested groups were very different from those for the non-transfected retina especially in the blind p23H retina (Fig. E2c), but the cumulative distribution of latencies further highlighted these differences (Fig. E2d). These results suggested a natural mechanosensitivity in photoreceptors highly reminiscent to that of auditive cells in agreement with the expression of Usher proteins in both sensory cells. These Usher proteins are known for generating the auditory mechanotransduction and likely the phototropism of photoreceptors underlying the Stiles Crawford effect[32].

MscL expression decreased latency and increased the mean number of cells per retina responding to US (Fig. 2h). Short latency (SL) responding cells expressing MscL were sensitive at much lower US pressures than non-transfected cells and their number increased with increasing US pressures (Fig. 2i). SL US responses also involved higher firing rates and were more sustained than LL US responses (Fig. 2j). Moreover, we observed that the G22S mutation further enhanced the sensitivity of SL RGCs to lower US pressures (Fig. 2k, E1b). We subsequently restricted our analyses to SL US responses (<45ms). Neurons responded to even very short stimulation durations (10 ms), with responses showing a fast return to the control level of activity (Fig. 3a). US response durations were correlated with stimulus duration although a reduction of the firing rate occurred for long stimuli (>100 ms) (Fig. 3c-d). Using different stimulus repetition rates, RGCs were able to follow rhythms up to a 10 Hz frequency (Fig. 3b-e). The Fano factor indicated that the response had a low variability in spike count and possibly high information content (Fig. 3c-e).

We then investigated whether different US frequencies (0.5, 2.25 and 15 MHz) affected the spatial resolution of the response, in accordance with the measured US pressure fields (Fig. E3). Transducers were designed with a similar focal distance and numerical aperture, for the transmission of focused beams over different frequency ranges (*0.5*, *2.25*, *15 MHz,* corresponding to wavelengths of 3.0, 0.7 and 0.1 mm, respectively) (Fig. 1c-e). Features of the responses evoked by the different US frequencies were found to be similar (Fig. E2e-f) although increasing the frequency from 0.5 MHz (typical of neuromodulation) (Fig. 1c) to 15 MHz (Fig. 1e) reduced the focal spot by a factor ~4100 with our transducers. Cells responding to US were widespread over the recorded area for 0.5 and 2.25 MHz, but appeared to be more confined for 15 MHz (Fig. 3f), despite similar acoustic parameters (100ms: 1.1 and 1.3 MPa) for the 2.25 MHz and 15 MHz beams. The acoustic pressure at 0.5 MHz was lower (0.5 MPa) due to electric power limitation of our electronics. The spatial dispersion of activated cells

decreased significantly from 1.48±0.12 mm and 1.30±0.18 mm at 0.5 MHz and 2.25 MHz, respectively, to 0.59±0.03 mm at 15 MHz (Fig. 3g). This spatial dispersion was consistent with the size of the measured ultrasound pressure fields (Fig. 1c-e); for the 0.5 MHz transducer, the focal spot was much larger than the MEA chip. The density of activated cells increased significantly with increasing US frequency but on a smaller area (Fig. 3h). US stimulation is more effective at higher frequencies, because lower acoustic power values are required to activate an equivalent number of cells. Indeed, even if the acoustic intensities at 2.25 and 15 MHz were quite similar, the acoustic power delivered was almost two orders of magnitude lower at 15 MHz (0.03 W) than at 2.25 MHz (0.82 W). At 15 MHz, moving the focal spot of the US probe above the retina triggered a shift in the area of responding cells (Fig. 3i). The response center was found to move in accordance with the displacement of the US transducer (Fig. 3j). These results demonstrate that our sonogenetic therapy approach can efficiently activate neurons with a millisecond and sub-millimetric precision.

Spatiotemporal resolution *in vivo* on the visual cortex

We investigated whether the approach could also be applied to the brain *in vivo* through a cranial window (Fig. 1a,b). As the G22S mutation enhanced the US sensitivity of RGCs *ex vivo*, we expressed MscL-G22S in cortical neurons of the primary visual cortex (V1) in rats. We injected AAV9.7m8 encoding the MscL-G22S channel fused to tdTomato under the control of the neuron-specific CamKII promoter into V1. TdTomato fluorescence was detected in the brain (Fig. 4a) and in cortical slices, particularly in layer 4 (Fig. 4b). Staining with an anti-NeuN antibody showed that 33.4% of cortical neurons in the transfected area expressed tdTomato (Fig. 4c).

To measure responses to 15MHz US Stimulations, we placed a micro-EcoG (µEcoG) electrode array on the cortical surface of V1 (Fig. 4d). In non-transfected (NT) animals, no US-evoked signal was recorded (Fig. 4e-right, *n*=3 rats), whereas, in V1 expressing MscL-G22S, US stimulation of the cortical surface elicited large negative µEcoG potentials (Fig. 4e-middle, *n*=6 rats). These US-evoked negative deflections were different from the recorded visual-evoked potentials (Fig. 4e-left). Amplitudes and durations of the US responses were clearly related to the duration of US stimulations (Fig. 4f, 4h) and US pressures (Fig. 4g). V1 cortical responses were again able to follow a repetition rate of up to 13 Hz (Fig. 4i) even if peak amplitude decreased slightly for increasing stimulation frequencies.

The peak depolarization of each channel was measured and linearly interpolated to build pseudocolor activation maps showing sizes of the US-responding cortical area dependent on the US pressure from 0.26 MPa (0.58 ± 0.17 mm^2 *n*=6 rats) to 1.27 MPa (1.41 ± 0.23 mm^2 *n*=5 rats) (Fig. 4j-l). When the ultrasound probe was moved laterally, the source of the generated neuronal activity moved in a similar direction (Fig. 4k). The spatial location of the evoked potentials moved by 0.29 mm (± 0.09 mm, *n*=6 rats) from the previous location (Fig. 4m, Fig. E5), even though we moved the US transducer in 0.4 mm steps. This discrepancy between the displacement of the activated area and movement of the transducer was certainly related to the 0.3 mm discrete spatial pitch distribution of the electrodes and the lateral spread of activity in the circuit. These results suggest that our approach to sonogenetic therapy could yield a spatial resolution of within 400 µm for stimulations at 15 MHz, the focal spot of our 15 MHz transducer being 276 µm wide (Fig. 1d). This opens up the possibility of targeting small areas (down to 0.58 mm^2 for 0.26 MPa), depending on the pressure level. These very localized US-evoked responses, their dependence on the position of the US probe and their short latencies confirmed that they were due to the activation of MscL-G22S-expressing neurons and not to an indirect response related to auditory activation, as previously suggested by others[33, 34].

When recording with penetrating electrode arrays (Fig. 4d), V1 neurons expressing MscL-G22S generated sustained responses even to 10 ms-long 15MHz US stimuli (Fig. 5a) with latencies shorter than 10ms (5.10 ± 0.62 ms n=27 cells) (Fig. 5b), consistent with a direct US activation. Responding neurons were recorded at various cortical depths, ranging from 100 µm to 1 mm (Fig. 5c), the focal spot diameter of the US probe being 3.75 mm in the xz plane. Deep neurons responded reliably to stimuli of decreasing duration, from 50 ms to 10 ms, with similar firing rates, whereas longer stimuli induced responses in a broader population of neurons (Fig. 5d-e). To investigate if an US pattern could be applied for visual restoration at a refreshing rate of up to 13 Hz, we increased progressively the sequence of stimuli. Cortical neurons were able to generate distinct responses to each US stimulus up to a 13 Hz repetition rate (Fig. 5f), but the number of responding cells decreased with increasing stimulus frequency (Fig. 5g). No major tissue temperature increase is expected even at this stimulation rate (Fig. E4).

Behavioral response to the sonogenetic stimulation of the visual cortex

To define if US-elicited synchronous activation of MscL-expressing excitatory cortical neurons can induce light perception, we assessed mouse behaviour during an associative learning test including 15 MHz US stimulation of V1 in MscL G22S-transfected (*n*=14) and non-transfected (*n*=9) animals (Fig. 6 and E6). Mice subjected to water deprivation were trained to associate the visible-light stimulation of one eye with a water reward (Fig. 6a)[35]. This task was learned within four days, as indicated by the increasing success rate during this period, from 30.9 ± 17.9% (SD) to 86.2 ± 14.1% (SD) for MscL-G22S-transfected mice (Fig. 6b). The success rate was determined by assessing the occurrence of an anticipatory lick between the light onset and the release of the water reward 500 ms later (Fig. 6a). Only mice reaching a 60% success rate on the 4th day were retained for this analysis and sessions showing a compulsive licking rate were excluded. Following cortical US stimulation on day 5, MscL-G22S-transfected mice achieved a success rate 69.3 ± 25.4 % (SD), the difference of which showed no statistical difference with the success rate following light stimulation on day 4 (Fig. 6b). After a pause during the weekend (day 6-7), the animals retained the task, their success rates showing no statistically significant differences with the one following light stimulation (Fig. 6b). By contrast, in non-transfected animals, the success rate following the US stimulation of their visual cortex dropped to 38.1 ± 18.5 % (SD), the difference with the success rate following light stimulation on the 4th day was highly significant (p<0.0001) (Figs 6d, E6). In the AAV-injected mice, we found that the latency of the first anticipatory lick was shorter for sonogenetic stimulation (187.1 ± 37.3 ms; *n*=14, SD) than for stimulation with a light flash (265.9 ± 46.5 ms; *n*=23, SD) (Fig. 6c, E6d). This shorter latency for the US response is consistent with the faster activation of cortical neurons for sonogenetic stimulation than for light stimulation of the eye (Fig. 4e). In transfected mice, success rates increased with pressure (Fig. 6d), suggesting a brighter and/or a larger US-elicited percept with a greater US pressure as described with increasing currents in human patients[4]. Interestingly, the licking frequency during the 500 ms before delivery of the water reward also increased with US pressure (Fig. 6e). These results suggest that the sonogenetic stimulation of the visual cortex generates a perception in mice that is likely associated to a visual perception although more complex visual behaviors as form discrimination would be required for a demonstration.

Safety issues

Our sonogenetic approach greatly decreased the US pressure required for the activation of RGCs and V1 cortical neurons with stimulation sequences remaining below FDA safety limits (510k, Track 3) for US imaging (e.g. for a 10 ms US stimulus of 0.6 MPa, the non-derated Isptp is 12 W/cm^2 and the non derated Ispta value is 0.12 W/cm^2). These very low acoustic pressures and acoustic intensities prevent tissue damage, as they are similar to those that have been widely used in clinical diagnostic imaging for decades[36]. Moreover, simulations of US-induced heating in brain tissue revealed that typical US parameters (i.e. 20 ms, 1.27 MPa) (Fig. 4e-h) increased the local temperature by an estimated 0.12 °C, with even high repetition rates (up to 13 Hz) leading to a moderate temperature increase (<0.3 °C) (Fig. E4c-f). These low-temperature fluctuations (corresponding to "worst-case" scenarios as we used non derated US parameters) and stimulation sequences compliant with FDA limits suggest that our approach had no toxic side effects and that US-elicited responses were not temperature-driven and were therefore probably mediated by mechanical activation of MscL channels by US. The fact that acoustics intensities and pressure used here remained far below the FDA requirements for conventional ultrasonic imaging in clinics (**https://www.fda.gov/media/71100/download**) and generated very low temperature increase in comparison with thermal damaging effects[37], raises high hopes for a smooth clinical translation. Moreover, a very recent safety study by Cheng et al[19] demonstrated an absence of brain tissue damages using high frequency activation at ten times higher acoustic intensities (continuous insonication at 11.8 W/cm2 compared to our "worst case" Ispta 1.56 W/cm2 for repeated stimulations at 13 Hz rate).

Conclusions

The development of remotely controlled cortical and subcortical deep neuronal stimulation techniques is of considerable interest for the treatment of diverse neurological diseases and sensory handicaps. Most previous sonogenetic studies focused on the use of low-frequency US[22-24] as in the recent demonstration of MscL-based sonogenetic activation in mouse brain[23]. However, such low-frequency US waves lead to limited centimetric spatial resolutions (~5x5x45 mm^3) and an uncontrolled spatial beam distribution. An alternative approach to spatially containing US stimulations involves the use of higher US frequencies, but this was thought to demand higher energy levels, exceeding safety limits and favoring tissue

damage[20]. The bacterial MscL channel has been reported to sensitize neurons to US[23, 27, 28] and to lower the pressure for neuronal activation, but its use for high-spatiotemporal resolution sonogenetic stimulation has yet to be shown to be effective *in vivo*. We here showed that that US activation of MscL-G22S expressed in retinal or cortical neurons resulted in responses with millisecond latencies and a spatial resolution of at least 400 µm in the *xy* plane at a 15 MHz frequency. The subsequent neuronal activation throughout the depth of the visual cortex (Fig. 5n-p) led to a behavioral motor response, suggesting light perception by the animal. These sonogenetic responses were genuinely related to MscL expression, as they were not observed in non-transfected animals. Following previous demonstrations that the MscL channel is a suitable sonogenetic actuator[23, 27, 28], we provide further evidence that the MscL channel has appropriate kinetics for the activation of neurons at a precise spatiotemporal resolution *in situ* and *in vivo*.

The temporal precision of sonogenetics is lower than that achieved with optogenetic (> 40Hz) by the fastest opsins[38] and ChrimsonR[39], which is successfully restoring vision at the retinal level in patients[6]. MscL only follows a 13 HZ frequency *in vivo*, which is in the same range as the 5-20 Hz achieved *in vivo* by the very sensitive opsin, ChRmine[40], a frequency range likely sufficient for vision[3]. The discovery of ChRmine has enabled investigators to stimulate deep into the rodent brain even from above the skull[40]. Future studies will have to examine the spatial resolution of this approach and how it compares to sonogenetics. As for all gene therapies in non-dividing cells, both optogenetic and sonogenetic therapies are expected to be life long lasting as indicated by gene therapy in congenital Leber amaurosis although it did not stop the ongoing degeneration of photoreceptors in patients[41].

Restoration of form vision at cortical level was previously achieved with 0.5 to 1 mm surface electrodes spaced more than 1 mm apart[5] or with 1.5-mm-long penetrating electrodes spaced 400 µm apart[4]. The spatial resolution of the proposed sonogenetic therapy therefore appears to be compatible with the cortical restoration of form vision but with a remote non-contact device. To preserve this spatiotemporal resolution, the ultrasound stimulator will require to be placed directly above the dura mater or above an ultrasound transparent artificial skull[42]. At 15 MHz, the typical penetration depth with negligible heating is typically 20 mm. Moreover, the resolution of the approach could be increased by using gene therapy to drive expression in specific cell populations and cell compartments[31, 43]. Further studies are required to generate an interface for coding visual information into US patterns transmitted

by an ultrasonic matrix array onto the visual cortex at a video rate. To reduce the ultrasound load, visual restoration can take advantage of event-based camera, heat-sensitive camera or depth filtering imaging to limit the active pixel number in an image[44-46]. Therefore, our approach provides great hope for the development of high-resolution visual restoration at the cortical level, through its unique combination of a rapid response, high spatial resolution, and cell selectivity with promoters. Even if this approach requires craniotomy, as for other existing visual prostheses, it provides a less invasive approach based on deep and distant cortical activation from above the dura mater following AAV cortical injections. More generally, it paves the way for a new type of genetic-based brain-machine interface capable of compensating for disabilities and suitable for use in treatments of neurological disorders.

Acknowledgements

The authors would like to thank C. Joffrois, M. Valet, Q. Cesar, M. Desrosiers, S. Fouquet, P. Annic, M. Celik, Z. Raics for technical help and scientific advice. This work was supported by the European Research Council (ERC) Synergy Grant Scheme (holistic evaluation of light and multiwave applications to high-resolution imaging in ophthalmic translational research revisiting the Helmholtzian synergies, ERC Grant Agreement #610110), by the European Union's Horizon 2020 research and innovation programme under grant agreement No. 785219 (Graphene Flagship Core 2) No. 881603 (Graphene flagship Core3), by the Foundation Fighting Blindness, La Fondation pour la Recherche Médicale (FRM EQUIPE EQU202106012159), l'UNIM, *la Fédération des Aveugles de France*, Optic 2000, the city of Paris, *Région ile de France*, the *Agence Nationale de la Recherche* (ANR BrainOptoSight), and French state funds managed by the *Agence Nationale de la Recherche* (ANR) within *Programme Investissements d'Avenir, Laboratoire d'Excellence* (LABEX) LIFESENSES (ANR-10-LABX-0065) and *Institut Hospitalo-Universitaire* FOReSIGHT (ANR-18-IAHU-0001), by NIH CORE Grant P30 EY08098 to the Department of Ophthalmology, the Eye and Ear Foundation of Pittsburgh, and from an unrestricted grant from Research to Prevent Blindness, New York, NY.

Author Contributions Statement

S.C., C.D. designed the experiments. I.A., M.P. contributed equally. S.C., M.P., G.L., I.A., J.L,

R.G., E.B., J.D. carried out the experiments and analyzed the data, M.P., D.N., G.G., F.A., O.M., D.D., M.S., B.R. provided support for experiments, study design and data analysis, S.P., M.T., J.S. conceived the idea for this project and supervised the analysis of the data obtained. S.C., C.D, I.A., M.T., S.P. wrote the manuscript. S.P. and M.T. contributed equally. All authors provided critical feedback on the research and the manuscript.

Competing interests Statement

The authors have filed for a patent for devices and methods for sonogenetic stimulation.

Tables: None

Figure Legends/Captions

Fig. 1 Sonogenetics using focused ultrasound beams for visual restoration through the intact dura mater: impact of ultrasonic transmision frequency. (a) Concept of visual restoration with US matrix arrays implanted in a cranial window for localized US neuromodulation of the primary visual cortex in humans. The US beam can be adaptively focused at different locations in the V1 cortex while passing through the intact dura mater, subdural and subarachnoid spaces. (b) Proof-of-concept setup used in this study for V1 sonogenetic activation in rodents, using a high-frequency focused transducer on a craniotomized mouse. (c) Characterization of the radiated field for the 0.5 MHz transducer used in this study. (top) Longitudinal view of the maximal pressure for a monochromatic acoustic field radiated at 0.5 MHz by the 25.4 mm Ø, 31.75 mm focus transducer. Pressure maximum is reached at 25.9 mm, slightly closer to the transducer than the geometric focal point, which is a documented effect [66]. (middle) Transverse section of the maximal pressure field at depth z = 25.9 mm. (bottom) One-dimensional profile of this transverse section giving the FWHM of the focal spot (4.36 mm at 0.5 MHz). (d) Same characterization for the 2.25 MHz 12.7mm Ø 25.4 mm focus transducer. (e) Same characterization for the 15 MHz 12.7mm Ø 25.4 mm focus transducer. Note that the maximum pressure is reached very close to the geometric focus (25.21 mm versus 25.4 mm for the geometric focus) for this configuration. The FWHM of the focal spot is 0.276 mm. Figures 1a and 1e were created with Biorender.com.

Fig. 2 Sonogenetic therapy in rat retinal ganglion cells. (a) *In vivo* retinal fundus image showing MscL-tdTomato expression. (b-c) Confocal stack projections across the retinal ganglion cell (RGC) layer of a flat-mounted retina. (d) Density of RBPMS-, MscL-positive and double-labeled cells (n=5 MscL WT and G22s retinas, *, p=0.0140, for RBPMS(+); *, p=0.0465, for RBPMS(+)/MscL(+), unpaired two-tailed t test). (e) Schematic diagram of the experimental setup with an image of the retina on MEA electrodes. (f) Representative peristimulus time histograms (PSTHs) for US or visual stimuli in MscL-transfected or non-transfected (NT) RGCs (US stimuli: 15 MHz, 1.27 MPa). (g) RGC response latencies to a 15 MHz US stimulus for MscL (n=300 cells, 9 retinas) and NT retinas (n=41 cells, 4 retinas). Dotted line: 45 ms latency threshold. (h) Number of cells per retina responding to 15 MHz US stimuli (0.98-1.27 MPa) for MscL (n=9 retinas) and NT (n=4 retinas) with short (< 45 ms, SL) or long latencies (> 45 ms, LL). * p=.0002, unpaired two-tailed t test. (i) Mean number of SL-responding RGCs per retina following stimulation with US stimuli of increasing pressure for MscL (n=9) and NT (n=4) retinas. *** p=0.00008, *** p=0.0010, *** p=0.0008, multiple unpaired two-tailed t test. (j) Maximum firing rate and response duration (of SL and LL RGCs from MscL retinas in response to US stimuli of increasing pressure (0.2-1.27 MPa) (n=9 retinas, ** p=0.0017, * p=0.0418, unpaired two-tailed t test). (k) Percentage of SL RGC cells (normalized against the maximum number of responsive cells in each experiment) responding to US stimuli for MscL WT (n=3 retinas) and MscL G22S (n=6 retinas) retinas. ** p=0.0065, ** p=0.0083, multiple unpaired two-tailed t test. (l) Ratios of RGCs responding to US stimulation with short (SL) or Long latencies (LL) for MscL and NT retinas (n=9 retinas for MscL and 4 for NT), following the application of a cocktail of synaptic blockers (CNQX-CPP-LAP4, n=3 retinas for both MscL and NT), and for P23H retinas with and without MscL expression (both n=3 retinas). * Conditions with no US-elicited cell responses. Data are presented as mean values +/- SEM. Scale bars represent 100, 20, 200μm in b,c,e.

Fig. 3 Spatiotemporal properties of sonogenetic retinal responses. (a-b) Spike density functions (SDFs) of two RGCs from a MscL retina for 15 MHz stimulus durations and repetition frequencies (a: 0.5 Hz repetition rate, b: 10, 20, 50, 200 ms durations). (c) Maximum firing rates for different 15 MHz stimulus durations and mean Fano factor values for all cells (10-20 ms n=8 retinas, 50-200 ms *n*=9 retinas). (d) Correlation between response duration and stimulus duration (*n*=9 retinas). (e) Maximum firing rates for different stimulus repetition frequencies and mean Fano factor values for all cells (0.2-2 Hz *n*=9 retinas, 5-10 Hz *n*=8 retinas). (f) (Top) Retinas on a MEA chip and corresponding size of the incident US pressure beam (circles represent the FWHM and are centered on the estimated center of response), for 0.5, 2.25 and 15 MHz. (Bottom) Corresponding activation maps representing the normalized firing rates of the cells following US stimulation. Each square box represents an electrode with at least one US-activated cell. (g) Spatial dispersion of activated cells and (h) ratio of the number of activated cells to the stimulated area for the three US frequencies, ****, p=0.00002 for panel g, p=0.00006 (15 vs 2.25 MHz) and p=0.00005 (15 vs 0.5 MHz) for panel h, ** p=0.0008, * p=0.0169, unpaired two-tailed *t* test. *N*=12 retinas for 0.5 MHz (0.29-0.68 MPa), *n*=5 retinas for 2.25 MHz (1.11-1.62 MPa), *n*=9 retinas for 15 MHz (1.12-1.27 MPa). (i) Heatmaps showing activated cells in a MscL retina following displacements (0.4 and 0.8 mm) of the US transducer. Circles represent the estimated center of the response. (j) Relative displacement of the center of the response following displacement of the 15 MHz US transducer. **** p=0.00001, ** p=0.0018, unpaired two-tailed *t* test. *n*=9, 9, and 6 positions for 4, 4 and 2 retinas for displacements of 0, 0.4 ± 0.20 and 0.8 ± 0.18 mm (SD), respectively. The dotted gray line represents the theoretical displacement. Data are presented as mean values +/- SEM. Scale bars represent 1 mm in f (top) and 0.5mm in f (bottom) and i.

Fig. 4 Spatial resolution of i*n vivo* sonogenetic therapy in V1 cortical neurons. (a) Image of a rat brain expressing MscL-G22S-tdTomato (red) in V1. (b) Confocal stack projection of a sagittal brain slice expressing MscL G22s-tdTomato (red) and labeled with anti-NeuN antibody (green) and DAPI (blue). The layers of V1 are delineated by dashed white lines. (Lower right) Magnification of layer 4 of V1. (c) Density of NeuN-positive, MscL-positive and double-labeled cells for 3 brain slices. (d) Schematic diagram of the setup used for *in vivo* electrophysiological recordings and US stimulation; (Top right) µEcoG electrode array placed on V1 of a MscL-transfected rat. (e) (Left) Visual-evoked cortical potentials in response to a 100 ms flash. (Middle) Sonogenetic evoked potentials for 15 MHz US stimuli of various durations. (Right) Absence of US responses on a non-transfected (NT) rat to a 15 MHz stimulus. Black traces represent the mean evoked potential over 100 trials, individually illustrated by the gray traces. The black arrow indicates the stimulus onset. (f) Duration of sonogenetic µEcog responses for stimuli of different durations (10 ms *n*=58, 20 ms n=32 and 50 ms n=56 trials on 6 animals). (g) N1 peak amplitude for increasing US pressure, (h) increasing duration and (i) frequency (*n*=6 rats). (j) Pseudocolor activation maps for stimuli of increasing US pressure and (k) for a horizontal displacement of the US transducer by 0.8 mm (the arrow indicates the direction of the displacement). Each black dot represents an electrode of the array. The color bar represents N1 peak amplitude in µV. (l) Mean activated area for various US pressure values (*n*=6 animals). (m) Relative displacement of the activation center to the previous position following movement of the US transducer by 0.4 mm. p=1 10^{-12}, one-sample two-tailed *t* test, *n*=37 positions on 6 animals (Mean: 0.29 ±: 0.16 mm, SD). Data are presented as mean values +/- SEM. Scale bars represent 200 and 50 µm in b, 300 µm in j-k.

Fig. 5: Temporal resolution of *in vivo* sonogenetic cortical activation. (a) Spike density functions (SDF) of 58 and 27 neurons recorded with a penetrating multielectrode array in MscL-transfected rats following US stimulation for 50 and 10 ms. (Red: mean trace, grey: individual cells) (b) Response latencies following 50 and 10 ms US stimuli (50 ms *n*=58 cells, mean: 7.5 ± 7.6 ms (SD), 7 rats; 10 msn=27 cells, mean: 5.1 ± 3.2 ms **(**SD), 5 rats). (c) Depth of US-responding cells (*n*=58) in MscL-expressing rats (*n*=7). (d) Instantaneous SDF of responses to US stimuli of different durations (1 Hz stimulus repetition frequency). (e) Maximum firing rates (n= 27, 22, 58 cells, SD: 55.8, 56.2, 49.8 ms for 10, 20 and 50 ms stimulation respectively) and numbers of activated neurons upon US stimulations of different durations (US pressure: 1 MPa). (f) Instantaneous SDF of responses to US stimuli of different repetition frequencies (10 ms stimulus duration). (g) Mean maximum firing rate and number of activated neurons upon US stimulation at different stimulus repetition frequencies (10 ms, 1MPa, n= 27, 40, 30, 10, 13 cells, SD: 55.8, 50.8, 55.7, 41.5, 58.2 Hz). Data are presented as mean values +/- SEM.

Fig. 6 Behavioural response induced by sonogenetic activation of the V1 cortex in mice following associative visual training. (a) Schematic diagram of the behavioral task performed by mice. Water-restricted animals trained in an associative learning paradigm for light stimulation (LS) with a water reward are subjected to either a light stimulation of the eye (day 1-4) or a US stimulation of V1 at 15 MHz (day 5 and 8-10). (b) Mean rates of successful trials for 4 days of training during learning of the association between light stimulation (LS, green, 50 ms) and water reward followed by the US stimulation (US orange, 1.2 MPa) for MscL-G22S transfected mice (between Day 4 LS and Day 5 US: 50 ms 1.2 MPa, ns p=0.0570. Between Day 5 US and Day 8 US: 50 ms 1.2 MPa, ns p=0.6079, two-tailed unpaired t test, Mean: 30.9, 49.9, 77.6, 86.2, 69.3, 62.3, 66.9, 76.5, SD: 17.9, 31.2, 13.9, 14.1, 25.4, 35.4, 37.1, 27.7%, n=14 animals) (c) Mean time to first lick after light (50 ms) and US stimulation (50 ms, 1.2 MPa) (**** p=0.0000290, two-tailed unpaired t test, n=23 and n=14 animals, Mean: 265.9, 187.1, SD: 46.5, 37.3 ms for LS and US respectively). (d) Mean rate of successful trials over 4 days of US stimulation for non-transfected (NT) and MscL-G22S transfected mice, following 50 ms of US stimulation at increasing US pressure (ns p=0.9452, *** p=0.0003, **** p=0.0000296, two-tailed unpaired t test, for 0.2, 0.7 and 1.2 MPa, respectively, n=14 animals, Mean: 35.2, 60.8, 68.7, SD: 17.5, 24.4, 23.6% for MscL-G22s; n=9 animals, Mean: 35.7, 27.5, 27.8, SD: 12.4, 11.0, 13.2% for NT). (e) Session anticipatory lick rates for NT and MscL-G22S transfected mice at increasing US pressures (ns p=0.6934, * p=0.0119, **** p=0.0000340, two-tailed unpaired t test, for 0.2, 0.7 and 1.2 MPa, respectively, n=14 animals, Mean: 1.4, 3.0, 4.1, SD: 0.4, 1.7, 1.8 Hz for MscL-G22S and n=9 animals, Mean: 1.3, 1.4, 1.2, SD: 0.3, 1.1, 0.5 Hz for NT). Data are presented as mean values +/- SEM.

References

1. Lebedev, M.A. & Nicolelis, M.A. Brain-Machine Interfaces: From Basic Science to Neuroprostheses and Neurorehabilitation. *Physiol Rev* **97**, 767-837 (2017).
2. Lewis, P.M., Ackland, H.M., Lowery, A.J. & Rosenfeld, J.V. Restoration of vision in blind individuals using bionic devices: a review with a focus on cortical visual prostheses. *Brain Res* **1595**, 51-73 (2015).
3. VanRullen, R. Perceptual Cycles. *Trends Cogn Sci* **20**, 723-735 (2016).
4. Fernandez, E. et al. Visual percepts evoked with an intracortical 96-channel microelectrode array inserted in human occipital cortex. *J Clin Invest* **131** (2021).
5. Beauchamp, M.S. et al. Dynamic Stimulation of Visual Cortex Produces Form Vision in Sighted and Blind Humans. *Cell* **181**, 774-783 e775 (2020).
6. Sahel, J.A. et al. Partial recovery of visual function in a blind patient after optogenetic therapy. *Nat Med* (2021).
7. Jazayeri, M., Lindbloom-Brown, Z. & Horwitz, G.D. Saccadic eye movements evoked by optogenetic activation of primate V1. *Nat Neurosci* **15**, 1368-1370 (2012).
8. Ju, N., Jiang, R., Macknik, S.L., Martinez-Conde, S. & Tang, S. Long-term all-optical interrogation of cortical neurons in awake-behaving nonhuman primates. *PLoS Biol* **16**, e2005839 (2018).
9. Chernov, M.M., Friedman, R.M., Chen, G., Stoner, G.R. & Roe, A.W. Functionally specific optogenetic modulation in primate visual cortex. *Proc Natl Acad Sci U S A* **115**, 10505-10510 (2018).
10. McAlinden, N. et al. Multisite microLED optrode array for neural interfacing. *Neurophotonics* **6**, 035010 (2019).
11. Legon, W. et al. Transcranial focused ultrasound modulates the activity of primary somatosensory cortex in humans. *Nat Neurosci* **17**, 322-329 (2014).
12. Tufail, Y. et al. Transcranial pulsed ultrasound stimulates intact brain circuits. *Neuron* **66**, 681-694 (2010).
13. Deffieux, T. et al. Low-intensity focused ultrasound modulates monkey visuomotor behavior. *Curr Biol* **23**, 2430-2433 (2013).
14. Lee, W. et al. Image-Guided Focused Ultrasound-Mediated Regional Brain Stimulation in Sheep. *Ultrasound Med Biol* **42**, 459-470 (2016).
15. Tufail, Y., Yoshihiro, A., Pati, S., Li, M.M. & Tyler, W.J. Ultrasonic neuromodulation by brain stimulation with transcranial ultrasound. *Nat Protoc* **6**, 1453-1470 (2011).
16. Legon, W., Bansal, P., Tyshynsky, R., Ai, L. & Mueller, J.K. Transcranial focused ultrasound neuromodulation of the human primary motor cortex. *Sci Rep* **8**, 10007 (2018).
17. Mehic, E. et al. Increased anatomical specificity of neuromodulation via modulated focused ultrasound. *PLoS One* **9**, e86939 (2014).
18. Kim, S. et al. Transcranial focused ultrasound stimulation with high spatial resolution. *Brain Stimul* **14**, 290-300 (2021).
19. Cheng, Z. et al. High resolution ultrasonic neural modulation observed via in vivo two-photon calcium imaging. *Brain Stimul* **15**, 190-196 (2022).
20. Ye, P.P., Brown, J.R. & Pauly, K.B. Frequency Dependence of Ultrasound Neurostimulation in the Mouse Brain. *Ultrasound Med Biol* **42**, 1512-1530 (2016).

21. Constans, C., Mateo, P., Tanter, M. & Aubry, J.F. Potential impact of thermal effects during ultrasonic neurostimulation: retrospective numerical estimation of temperature elevation in seven rodent setups. *Phys Med Biol* **63**, 025003 (2018).
22. Yang, Y. et al. Sonogenetics for noninvasive and cellular-level neuromodulation in rodent brain. *bioRxiv* **https://doi.org/10.1101/2020.01.28.919910** (2020).
23. Qiu, Z. et al. Targeted Neurostimulation in Mouse Brains with Non-invasive Ultrasound. *Cell Rep* **32**, 108033 (2020).
24. Huang, Y.S. et al. Sonogenetic Modulation of Cellular Activities Using an Engineered Auditory-Sensing Protein. *Nano Lett* **20**, 1089-1100 (2020).
25. Wu, X. et al. Sono-optogenetics facilitated by a circulation-delivered rechargeable light source for minimally invasive optogenetics. *Proc Natl Acad Sci U S A* (2019).
26. Yang, Y. et al. Sonothermogenetics for noninvasive and cell-type specific deep brain neuromodulation. *Brain Stimul* **14**, 790-800 (2021).
27. Ye, J. et al. Ultrasonic Control of Neural Activity through Activation of the Mechanosensitive Channel MscL. *Nano Lett* **18**, 4148-4155 (2018).
28. Soloperto, A. et al. Mechano-sensitization of mammalian neuronal networks through expression of the bacterial large-conductance mechanosensitive ion channel. *J Cell Sci* **131** (2018).
29. Sukharev, S.I., Blount, P., Martinac, B., Blattner, F.R. & Kung, C. A large-conductance mechanosensitive channel in E. coli encoded by mscL alone. *Nature* **368**, 265-268 (1994).
30. Dalkara, D. et al. In vivo-directed evolution of a new adeno-associated virus for therapeutic outer retinal gene delivery from the vitreous. *Sci Transl Med* **5**, 189ra176 (2013).
31. Chaffiol, A. et al. A New Promoter Allows Optogenetic Vision Restoration with Enhanced Sensitivity in Macaque Retina. *Mol Ther* **25**, 2546-2560 (2017).
32. Verschueren, A. et al. Planar polarity in primate cone photoreceptors: a potential role in Stiles Crawford effect phototropism. *Commun Biol* **5**, 89 (2022).
33. Sato, T., Shapiro, M.G. & Tsao, D.Y. Ultrasonic Neuromodulation Causes Widespread Cortical Activation via an Indirect Auditory Mechanism. *Neuron* **98**, 1031-1041 e1035 (2018).
34. Guo, H. et al. Ultrasound Produces Extensive Brain Activation via a Cochlear Pathway. *Neuron* **98**, 1020-1030 e1024 (2018).
35. Nelidova, D. et al. Restoring light sensitivity using tunable near-infrared sensors. *Science* **368**, 1108-1113 (2020).
36. ter Haar, G. Ultrasound bioeffects and safety. *Proc Inst Mech Eng H* **224**, 363-373 (2010).
37. Sapareto, S.A. & Dewey, W.C. Thermal dose determination in cancer therapy. *Int J Radiat Oncol Biol Phys* **10**, 787-800 (1984).
38. Aravanis, A.M. et al. An optical neural interface: in vivo control of rodent motor cortex with integrated fiberoptic and optogenetic technology. *J Neural Eng* **4**, S143-156 (2007).
39. Klapoetke, N.C. et al. Independent optical excitation of distinct neural populations. *Nat Methods* **11**, 338-346 (2014).
40. Chen, R. et al. Deep brain optogenetics without intracranial surgery. *Nat Biotechnol* **39**, 161-164 (2021).

41. Daich Varela, M., Cabral de Guimaraes, T.A., Georgiou, M. & Michaelides, M. Leber congenital amaurosis/early-onset severe retinal dystrophy: current management and clinical trials. *Br J Ophthalmol* **106**, 445-451 (2022).
42. Flores, A.R. et al. Safety, Feasibility, and Patient-Rated Outcome of Sonolucent Cranioplasty in Extracranial-Intracranial Bypass Surgery to Allow for Transcranioplasty Ultrasound Assessment. *World Neurosurg* **144**, e277-e284 (2020).
43. Greenberg, K.P., Pham, A. & Werblin, F.S. Differential targeting of optical neuromodulators to ganglion cell soma and dendrites allows dynamic control of center-surround antagonism. *Neuron* **69**, 713-720 (2011).
44. Lorach, H. et al. Artificial retina : The multichannel processing of the mammalian retina achieved with a neuromorphic asynchronous light acquisition device. *j Neural Eng* **9**, 066004 (2012).
45. Kartha, A. et al. Prosthetic Visual Performance Using a Disparity-Based Distance-Filtering System. *Transl Vis Sci Technol* **9**, 27 (2020).
46. Montezuma, S.R. et al. Improved localisation and discrimination of heat emitting household objects with the artificial vision therapy system by integration with thermal sensor. *Br J Ophthalmol* **104**, 1730-1734 (2020).

Methods

Animals

Experiments were conducted in accordance with the National Institutes of Health Guide for the Care and Use of Laboratory Animals. Protocols were approved by the Local Animal Ethics Committee (Committee Charles Darwin no. 5, registration number 9529 and 26889) and conducted in agreement with Directive 2010/63/EU of the European Parliament. Long Evans male rats aged between 2 and 12 months and wild-type male mice (C57BL/6J) aged 9 weeks were obtained from Janvier Laboratories, P23H (line 1) male transgenic rats (9-22 months) were raised locally.

Plasmid cloning & AAV production

Plasmids containing the *Escherichia coli mscL* sequence in the WT form and with the G22S mutation were obtained from Francesco Difato (Addgene plasmids #107454 and #107455)[28]. To target retinal ganglion cells, the SNCG promoter[31] was inserted into an AAV backbone plasmid containing the *mscL* sequence fused to the tdTomato gene and the Kir2.1 ER export signal, to drive expression at the plasma membrane. An AAV2.7m8 vector was used for intravitreous delivery. For targeting neurons in V1 cortical layers, the SNCG promoter was replaced by the CamKII promoter and an AAV9.7m8 vector was chosen. Recombinant AAVs were produced by the plasmid cotransfection method, and the resulting lysates were purified by iodixanol purification[31].

US stimulus

Three focused ultrasound transducers with different central frequencies were used: 0.5 MHz (diameter Ø = 1 inch = 25.4mm, focal distance f = 1.25 inch = 31.7 mm) (V301-SU, Olympus), 2.25 MHz (Ø = 0.5 inch = 12.7 mm, f = 1 inch = 25.4 mm) (V306-SU, Olympus) and 15 MHz (Ø = 0.5 inch = 12.7 mm, f = 1 inch = 25.4 mm) (V319-SU, Olympus), corresponding to numerical apertures F/Ø= 1,25 and 2. Acoustic fields radiated by those three focused transducers are presented in Figure 1 (simulations) and extended figure E3 (experimental measurements). A TiePie Handyscope (HS5, TiePie Engineering) was used to produce the stimulus waveform, which was then passed through an 80 dB RF power amplifier (VBA 230-80, Vectawave) connected to the transducer. Transducer pressure outputs (pressure at focus, 3D pressure

maps) were measured in a degassed water tank with a Royer-Dieulesaint heterodyne interferometer[47]. US stimuli used for *ex vivo* and *in vivo* stimulation had the following characteristics: 1 kHz pulse repetition frequency with a 50% duty cycle, sonication duration between 10 and 200 ms and inter-stimulus interval between 0.01 and 2 s. Peak acoustic pressures were ranging from 0.11-0.88 MPa, 0.3-1.6 MPa, 0.2-1.27 MPa, for the 0.5, 2.25 and 15 MHz transducers, respectively. The corresponding estimated Isppa values were 0.39-25.14 W/cm^2, 2.92-83.12 W/cm^2 and 1.30-52.37 W/cm^2.

Intra-vitreal gene delivery and retinal imaging

Rats were anesthetized[48] and AAV suspension (2 µl), containing between 8 and 14 x 10^{10} viral particles, was injected into the center of the vitreous cavity. One month later, tdTomato fluorescence imaging was performed on the injected eyes, with a Micron IV retinal imaging microscope (Phoenix Research Laboratories) and Micron Discover V2.2.

MEA recordings

Retinal pieces were flattened on a filter membrane (Whatman, GE Healthcare Life Sciences) and placed on a poly-L-lysine (0.1%, Sigma) coated multi-electrode array (electrode diameter 30 µm, spacing 200 µm, MEA256 200/30 iR-ITO, MultiChannel Systems) with RGCs facing the electrodes[31]. AMPA/kainate glutamate receptor antagonist 6-cyano-7-nitroquinoxaline-2,3-dione (CNQX, 25 µM, Sigma-Aldrich), the NMDA glutamate receptor antagonist [3H]3-(2-carboxypiperazin-4-yl) propyl-1-phosphonic acid (CPP, 10 µM, Sigma- Aldrich) and a selective group III metabotropic glutamate receptor agonist, L-(+)-2-amino-4-phosphonobutyric acid (L-AP4, 50 µM, Tocris Bioscience), were bath-applied through the perfusion line. Light stimuli were delivered with a digital micro-mirror display (DMD, Vialux, resolution 1024x768) coupled to a white LED light source (MNWHL4, Thorlabs) focused on the photoreceptor plane (irradiance 1 $\mu W/cm^2$). US transducers were coupled with a custom-made coupling cone filled with degassed water, mounted on a motorized stage (PT3/M-Z8, Thorlabs) placed orthogonally above the retina. The reflected signal of the MEA chip and the retina was detected with an US-key device (Lecoeur Electronique). The distance between the retina and the transducer was equal to the focal length of the transducer; this was verified with the flight time of the reflected signal. From RGC recordings with a 252-channel preamplifier and MC_Rack V4.6.2 (MultiChannel Systems), spikes were sorted with SpykingCircus 0.5

software[49]. RGC responses were analyzed with custom scripts written in Matlab (MathWorks 2018b) for classification as ON, ON-OFF or OFF, with the response dominance index[50]. Latencies were calculated as the time between stimulus onset and the maximum of the derivative of spike density function. Two classes of US-responding cells were identified on the basis of latency — short and long latency — by fixing a threshold equal to the minimum of the latency distribution of the responses of non-transfected cells to US (45 ms). We determined the peak value A of spike density function for the calculation of response duration, which was defined as the time interval between the two time points for which the SDF was equal to A/*e* (*e*: Euleur's number). The Fano factor, quantifying spike-count variability, was calculated as the ratio of the variance of the spike-count to the mean. The Euclidean distance between two activated cells was weighted according to the maximum firing rate of the cells. The ratio of the number of activated cells to the size of the area stimulated on the MEA chip was calculated considering the size of the US focal spot for 2.25 and 15 MHz and the size of the MEA for 0.5 MHz, because the focal spot was larger than the MEA for this frequency. The center of the response was estimated by weighting the maximum firing rate of each cell by its distance from other responding cells, and the displacement of the response was calculated as the Euclidean distance between two center-of-response positions.

Intracranial injections

AAV suspensions were injected into the right hemisphere at two different locations in rats (2.6 mm ML, 6.8 mm AP and 3.1 mm ML, 7.2 mm AP from bregma) or at one location in mice (2.5 mm ML, 3.5 mm AP from bregma)[48]. For rat injection, the suspension (200 nl, containing 0.2-8 x 10^{15} viral particles) was injected at three different depths (1100, 1350 and 1500 µm DV) with a micro-syringe pump controller (Micro4, World Precision Instruments) operating at a rate of 50 nl/min and a 10 µl Hamilton syringe. In mice, AAV suspension (1 µl containing 0.2-8 x 10^{15} viral particles) was injected at -400 µm DV at a rate of 100 nL/min.

***In vivo* extracellular recordings**

One month after AAV injections, a small craniotomy (5x5 mm square) was drilled above V1 in the right hemisphere[48]. TdTomato fluorescence was checked with a Micron IV retinal imaging microscope and Micron Discoverer V2.2 (Phoenix Research Laboratories). A 32-site µEcog electrode array (30 µm electrode diameter, 300 µm electrode spacing, FlexMEA36,

MultiChannel Systems) was positioned over the transfected region or in a similar zone for control rats. Multi-electrode (MEA) recordings were performed with a 16-site silicon microprobe tilted at 45° to the brain surface (electrode diameter 30 µm, spacing 50 µm, A1x16-5mm-50-703, NeuroNexus Technologies) and MC_Rack V4.6.2. The MEA was advanced 1100 µm into the cortex with a three-axis micromanipulator (Sutter Instruments, Novato, CA). US transducers were coupled to the brain with a custom-made coupling cone filled with degassed water and US gel on a motorized stage. The distance between the cortex and the transducer was equal to the focal length of the transducer. Visual stimuli were generated by a white light-collimated LED (MNWHL4, Thorlabs) placed 15 cm away from the eye (4.5 mW/cm^2 at the cornea). Recordings were digitized with 32- and 16-channel amplifiers (model ME32/16-FAI-µPA, MultiChannel Systems). µEcog recordings were analyzed with custom-developed Matlab scripts, MEA recordings with SpykingCircus software and custom-developed Matlab scripts. Response duration was calculated as the interval between the two time points at which the cortical evoked potential was equal to A/*e* (where A is peak depolarization and *e* is Euleur's number). The activated area was defined as the area of the pseudocolor activation map over which peak depolarization exceeded the background noise level calculated as 2 times the standard deviation of the signal. The response center was estimated by weighting the peak depolarization of each electrode by its distance from other electrodes. Its relative displacement when moving the US transducer, was calculated as the Euclidean distance of the two positions. For intracortical recordings, cell latency was estimated as the time between stimulus onset and the maximum of the derivative of spike density function.

Surgery for *in vivo* behavioral testing

C57BL6J mice were injected subcutaneously with Buprenorphine (0,05 mg/kg) (Buprécare, Axience), and Dexamethasone (0,7 mg/kg) (Dexazone, Virbac). Animals were anesthetized with Isoflurane (5% induction, 2% maintenance, in air/oxygen mixture) and the head was shaved and cleaned with antiseptic solution. Animals were head-fixed on a stereotactic frame with an Isoflurane delivering system, eye ointment and a black tissue were applied over the eyes. Body temperature was maintained at 37°C. After a local injection of Lidocaïne (4 mg/kg) (Laocaïne, Centravet), an incision of the skin was made. Two screws were fixed in the skull, after a small craniotomy (approximately 5 mm x 5 mm) was drilled above V1 in the right

hemisphere (0.5 mm steel drill) and cortex buffer was applied. The cortex was covered with a TPX plastic sheet (125 µm thick) and sealed with dental acrylic cement (Tetric Evoflow). For behavioral experiments, a metallic headbar (Phenosys) for head fixation was then glued to the skull on the left hemisphere with dental cement (FUJUCEM II). Animals were placed in a recovery chamber, with subcutaneous injection of physiological serum and ointment on the eyes (Ophtalon, Centravet). Buprenorphine was injected during post-surgery monitoring.

Mouse behavioral tests

Mice were placed on a water restriction schedule until they reached approximately 80-85% of their weightFollowing habituation to the test conditions[35], mice were trained to respond to a light stimulus by performing a voluntary detection task: licking a waterspout (blunt 18G needle, approximately 5 mm from mouth) in response to white light full-field stimulation (200 and 50 ms long) of the left eye (dilated with tropicamide, Mydriaticum Dispersa) 35 trials per stimulation duration so 70 trials per day. Water (~4 µL) was automatically dispensed 500 ms after the light was switched on, through a calibrated water system. The behavioral protocol and lick detection were controlled by a custom-made system[35]. The next four days (two-day break during the weekend), US stimulations were delivered on V1 for 50 ms at three different pressure values (0.2, 0.7 and 1.2 MPa). These pressure values were delivered in a different order each day (35 trials each). Inter-trial intervals varied randomly and ranged between 10 and 30 s. The 15 MHz US transducer was coupled to the brain with a custom-made coupling cone filled with water and US gel. The success rate was calculated by counting the number of trials in which mice performed anticipatory licks (between stimulus onset and the opening of the water valve). The session anticipatory lick rate shown in Fig. 6e was calculated by subtraction from the anticipatory lick rate of a trial, the spontaneous lick rate (calculated on all the 1 s time windows before each individual stimulus onset (see figure 6a) for all trials) and multiplication by the success rate. Lick latency was calculated by determining the time to the first anticipatory lick after stimulus onset. Mice retained for analysis presented a success rate superior or equal to 60% on the 4th day following light stimulation (LS). Then, Light or US sessions showing a compulsive licking behaviour were excluded based on the outlier identification made using ROUT method (Q = 1%) on the session spontaneous lick rate averaging the measurements on all the trials of the session in the 1s time window before the stimulus onset of the trial.

Immunohistochemistry and confocal imaging

Samples were incubated overnight at 4 °C with a monoclonal anti-RBPMS antibody (1:500, Rabbit, ABN1362, Merck Millipore) for the retina[31], with a monoclonal anti-NeuN antibody (1:500; Mouse, clone A60, MAB377, Merck Millipore) for brain sections[48]. The sections were then incubated with secondary antibodies conjugated with Alexa Fluor 488 (1:500; Donkey anti-Mouse and Donkey anti-Rabbit IgG 488, polyclonal, A-21202 and A-21206, Invitrogen) and DAPI (1:1000, D9542, Merck Millipore) for 1 h at room temperature. An Olympus FV1000 confocal microscope with 20x objective (UPLSAPO 20XO, NA: 0.85) was used to acquire images of flat-mounted retinas and brain sections (Software FV10-ASW V04.02).

On confocal images processed with FIJI (ImageJ 1.53q), RBPMS- and NeuN-positive cells were counted automatically with the *Analyze particles* FIJI plugin. Cells were counted manually by two different users, with the CellCounter FIJI plugin. Quantification was performed by acquiring confocal stacks in at least four randomly chosen transfected regions of 0.4 mm^2 (Fig. E1). For V1 neurons, the sagittal brain slice with the largest tdTomato fluorescence zone was selected for each animal. A ROI in V1 was manually defined and quantifications were performed in at least six randomly chosen regions of 0.4 mm^2.

US-induced tissue-heating simulations

A three-fold process was used for the estimation of thermal effects: 1) simulation of the acoustic fields generated by the three transducers, with realistic acoustic parameters, 2) verification that non-linear acoustics did not play an important role in heat transfer and 3) realistic simulations of heat transfer and temperature rise induced at the focus by US in a linear regime for parameters used in this study.

For non-linear simulations, we used Matlab's toolbox *kWave*, by defining the geometry of the transducer in 3D, and using the following parameters for the propagation medium (water): sound speed $c = 1500$ m s^{-1}, volumetric mass $\rho = 1000$ kg m^{-3}, non-linearity coefficient B/A = 5, attenuation coefficient α = 2.2 10^{-3} dB cm^{-1} MHz^{-y}, and frequency power law of the attenuation coefficient y = 2 [51]. We simulated quasi-monochromatic 3D wave-fields using long bursts of 50 cycles; this gave us both the maximum pressure field in 3D and the waveform at the focus. Simulations were calibrated by adjusting the input pressure (excitation of the simulated transducer) to reach the pressure at the focus measured in the water tank with the

real transducers. The FWHM focal spot diameter in the *xy* plane was 4.36, 1.61 and 0.276 mm, and the major axis in the *xz* plane was 32.3, 20.6 and 3.75 mm long for the 0.5, 2.25 and 15 MHz transducers, respectively (Fig. 1b-d). Non-linear effects were evaluated by estimating the relative harmonic content of the waveform at the focus. In the 15 MHz focus transducer example in figure 1d, the experimental and simulated signals at the focal spot were compared and found to be highly concordant (Fig. E4a). Furthermore, the amplitude of the second harmonic is 19.8 dB below the fundamental (20.9 dB in the simulated case), meaning that if the fundamental energy is E, the second harmonic has energy E/95 (Fig. E4b). Therefore, we can reasonably neglect the non-linear effects in the calculations of the thermal effects, as they account for ~1% of the energy involved. The same conclusions were drawn at 0.5 MHz and 15 MHz. Linear wave propagation approximations considerably decreased the computing cost of the simulations. Linear propagation simulations were conducted with the *Field II* toolbox in Matlab[52, 53], in monochromatic mode, with the same medium properties as *kWave* (water), to obtain the 3D maximum pressure fields. These maximum pressure fields were used to build a heating source term $Q_{US} = \frac{\alpha_{np} p_{max}^2}{\rho_b c_b}$, where α_{np} is the absorption coefficient of the brain at the considered frequency (59.04 Np m^{-1} at 15 MHz, calculated from α_{brain} = 0.21 dB cm^{-1} MHz^{-y} and y = 1.18), the brain volumetric mass ρ_{brain} = 1046 kg m^{-3}, the brain sound speed $c_{brain} =$ 1546 m s^{-1} [61,64], and p_{max} is the 3D maximum pressure field. This source term was then used in the resolution of a Penne's bioheat equation $\rho_{brain} C_{brain} . \frac{\partial T}{\partial t} = div(K_t . \nabla T) - \rho_{blood} C_{blood} P_{blood} (T - T_a) + Q$ in *kWave*, where C_{brain} is the blood specific heat capacity (3630 J.kg^{-1} °C^{-1}), K_t the brain thermal conductivity (0.51 W.m^{-1} °C^{-1}), ρ_{blood} the blood density 1050 kg m^{-3}, C_{blood} the blood specific heat capacity (3617 J.kg^{-1} °C^{-1}), P_{blood} the blood perfusion coefficient (9.7 10^{-3} s^{-1}), T_a the arterial temperature (37°C), and $Q = Q_{US} + \rho_{brain} . \gamma_{brain}$ with γ_{brain} the heat generation of the brain tissue (11.37 W kg^{-1}) [54, 55]. The initial condition for brain temperature was set to $T_0 = 37$ °C.

This simulation corresponds to the worst-case scenario regarding the temperature rise given: 1) that the acoustic propagation is simulated in water only (non derated value), with a lower attenuation coefficient (2.2 10^{-3} dB cm MHz^{-2}) than the brain (0.59 dB cm MHz$^{-1.27}$), even if a part of the propagation occurs within the brain. p_{max} maps are, therefore, overestimated. 2) thermal absorption is simulated in brain tissue only, with a higher absorption coefficient (0.21

dB cm $MHz^{-1.18}$) than water, even if a part of the maximum pressure field is actually located within the water of the acoustic coupling cone. Q_{US} is, therefore, slightly overestimated. We mapped the temperature in three spatial dimensions and time, and looked for the point of maximal temperature rise (Fig. E4 c-f).

Statistical analysis

Statistical analyses were carried out with Prism software (Prism 9, GraphPad). Values are expressed and represented as means ± the standard error of the mean (SEM) on figures and in the text unless specified. Data were analyzed in unpaired Welch's *t*-tests (two-tailed) or an unpaired multiple *t*-tests with Sidak- Bonferroni correction for multiple comparisons. Statistical tests are provided in figure legends.

Data availability

Data supporting the findings of this study are available within the paper and Supplementary information as well as on FigShare : https://figshare.com/projects/Ectopic_expression_of_a_mechanosensitive_channel_confers_spatiotemporal_resolution_to_ultrasound_stimulations_of_neuronal_circuits_for_visual_restoration/154041.

All other data are available from the corresponding author upon reasonable request.

Code availability

The custom Matlab codes are available from the corresponding author upon request.

Methods-only references

47. Royer, D. & Dieulesaint, E. Optical probing of the mechanical impulse response of a transducer. . *Applied Physics Letters* **49**, 1056–1058 (1986).
48. Provansal, M. et al. Functional ultrasound imaging of the spreading activity following optogenetic stimulation of the rat visual cortex. *Sci Rep* **11**, 12603 (2021).
49. Yger, P. et al. A spike sorting toolbox for up to thousands of electrodes validated with ground truth recordings in vitro and in vivo. *Elife* **7** (2018).
50. Akerman, C.J., Smyth, D. & Thompson, I.D. Visual experience before eye-opening and the development of the retinogeniculate pathway. *Neuron* **36**, 869-879 (2002).
51. Duck, F.A. A. Physical Properties of Tissues: A Comprehensive Reference Network. , (Academic Press,). *Ultrasound in Medicine & Biology* **36**, (Academic Press) (1990).

52. Jensen, J.A. & Svendsen, N.B. Calculation of pressure fields from arbitrarily shaped, apodized, and excited ultrasound transducers. *IEEE Trans Ultrason Ferroelectr Freq Control* **39**, 262-267 (1992).
53. Jensen, J.A. A Program for Simulating Ultrasound Systems. *Medical & Biological Engineering & Computing* **34**, 351-353 (1996).
54. DATABASE., I.F. Available at: https://itis.swiss/virtual-population/tissue-properties/database. (Accessed: 17th August 2020).
55. McIntosh, R.L. & Anderson, V.A. A comprehensive tissue properties database provided for the thermal assessment of a human at rest. *Biophysical Reviews and Letters* **5**, 129–151 (2010).

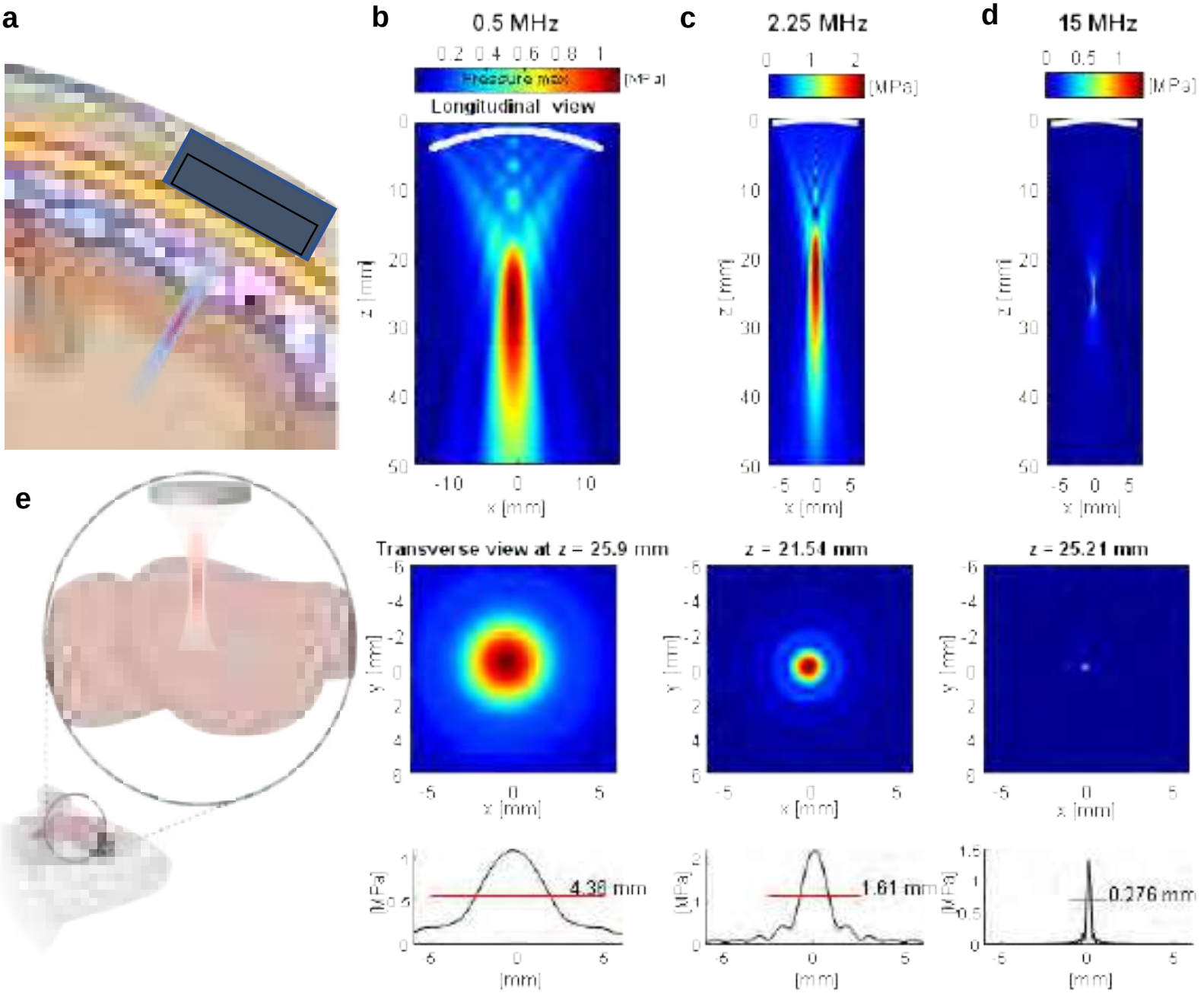
a
b
0.5 MHz
0.2 0.4 0.6 0.8 1
Pressure max
[MPa]
Longitudinal view
z [mm]
x [mm]
c
2.25 MHz
0 1 2
[MPa]
d
15 MHz
0 0.5 1
[MPa]
e
Transverse view at z = 25.9 mm
z = 21.54 mm
z = 25.21 mm
y [mm]
x [mm]
[MPa]
4.38 mm
1.61 mm
0.276 mm
[mm]

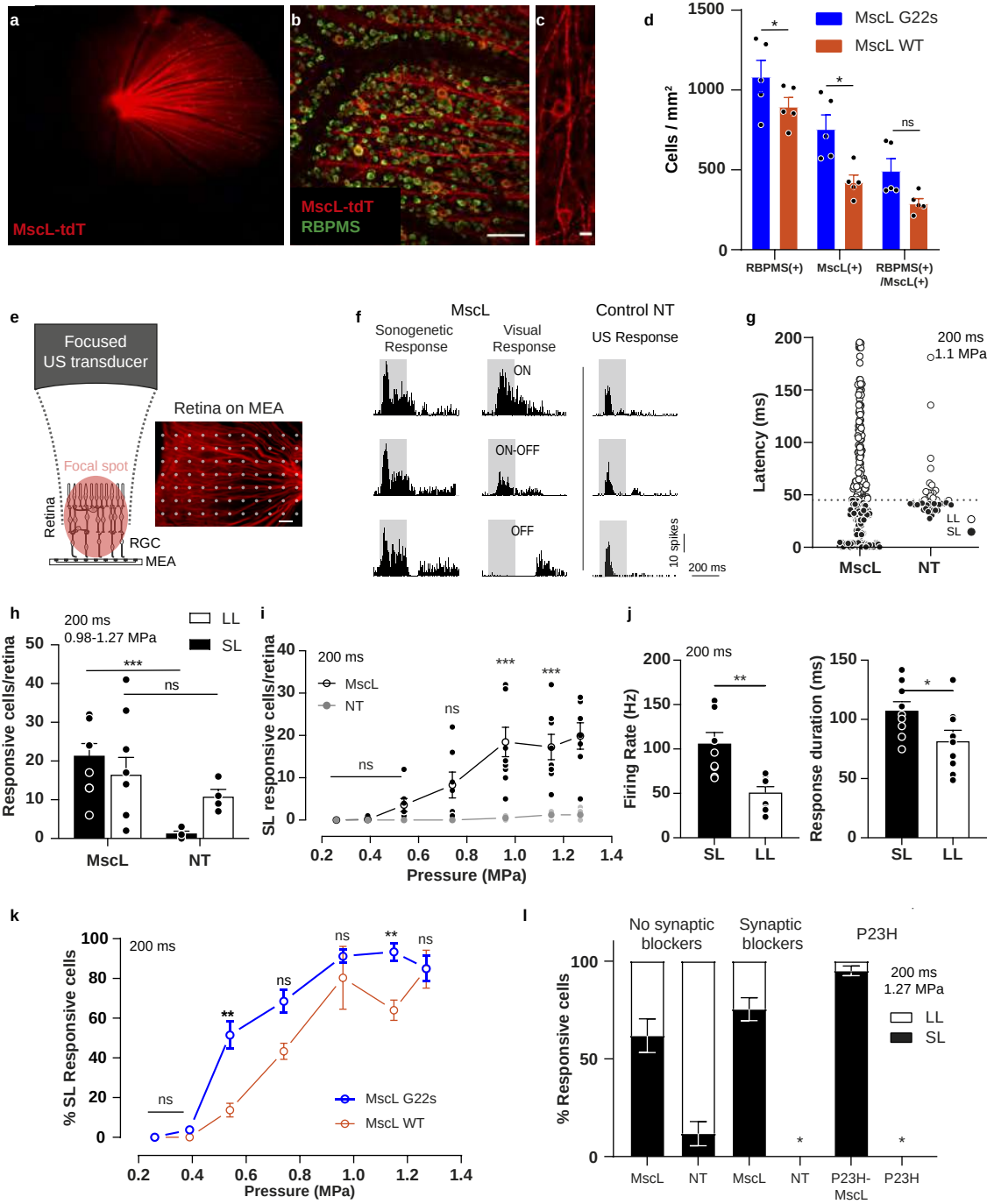
a
MscL-tdT
b
MscL-tdT
RBPMS
c
d
Cells / mm²
MscL G22s
MscL WT
RBPMS(+)
MscL(+)
RBPMS(+) /MscL(+)
ns
e
Focused US transducer
Retina on MEA
Focal spot
Retina
RGC
MEA
f
MscL
Control NT
Sonogenetic Response
Visual Response
US Response
ON
ON-OFF
OFF
10 spikes
200 ms
g
Latency (ms)
200 ms
1.1 MPa
LL
SL
MscL
NT
h
200 ms
0.98-1.27 MPa
LL
SL
Responsive cells/retina
MscL
NT
i
200 ms
MscL
NT
SL responsive cells/retina
Pressure (MPa)
j
200 ms
Firing Rate (Hz)
Response duration (ms)
SL
LL
k
200 ms
% SL Responsive cells
MscL G22s
MscL WT
Pressure (MPa)
l
No synaptic blockers
Synaptic blockers
P23H
200 ms
1.27 MPa
LL
SL
% Responsive cells
MscL
NT
MscL
NT
P23H-MscL
P23H

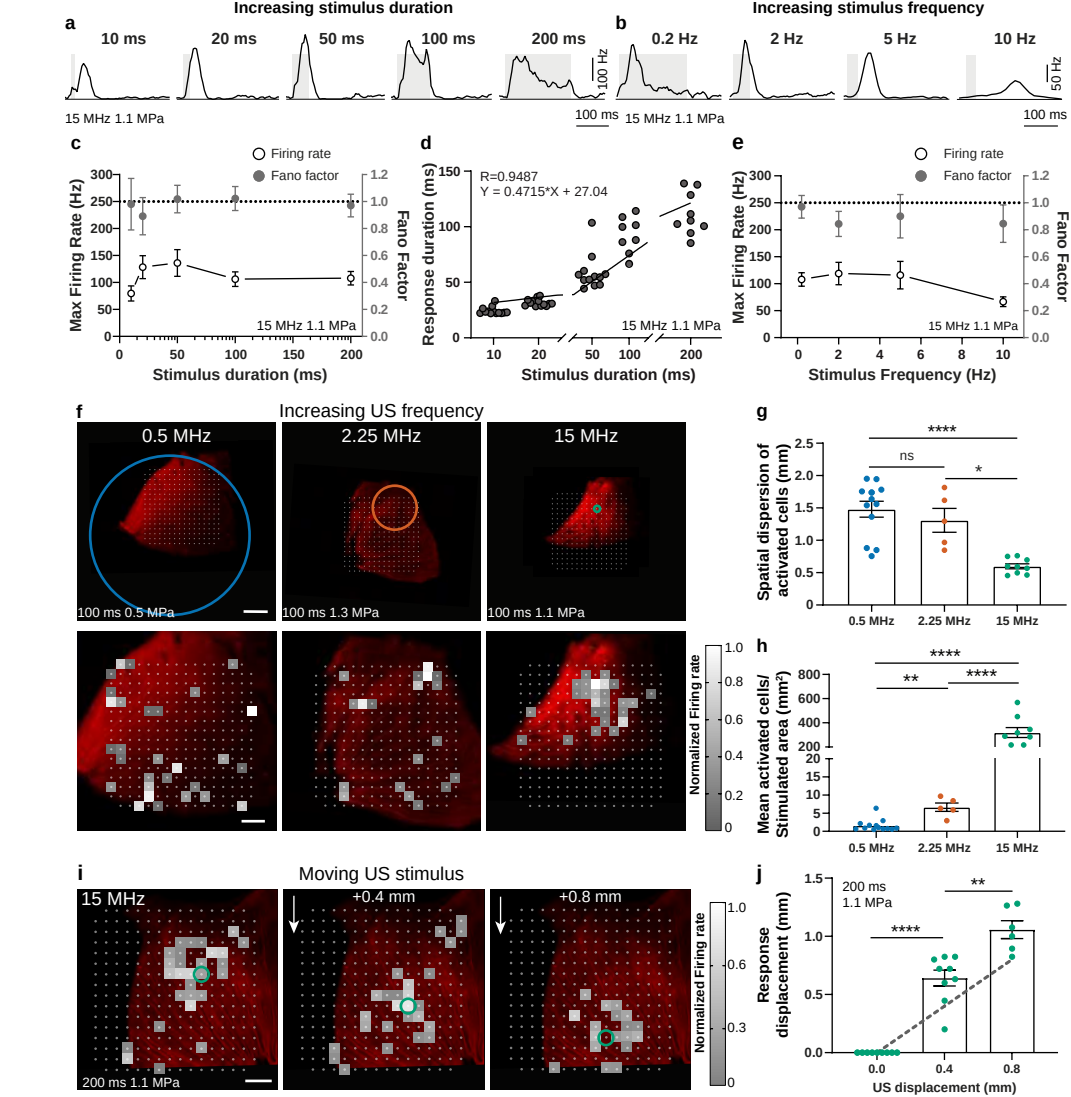
a
Increasing stimulus duration
10 ms
20 ms
50 ms
100 ms
200 ms
100 Hz
15 MHz 1.1 MPa
100 ms
b
Increasing stimulus frequency
0.2 Hz
2 Hz
5 Hz
10 Hz
10 Hz
15 MHz 1.1 MPa
100 ms
c
Firing rate
Fano factor
Max Firing Rate (Hz)
Fano Factor
15 MHz 1.1 MPa
Stimulus duration (ms)
d
R=0.9487
Y = 0.4715*X + 27.04
Response duration (ms)
15 MHz 1.1 MPa
Stimulus duration (ms)
e
Firing rate
Fano factor
Max Firing Rate (Hz)
Fano Factor
15 MHz 1.1 MPa
Stimulus Frequency (Hz)
f
Increasing US frequency
0.5 MHz
2.25 MHz
15 MHz
100 ms 0.5 MPa
100 ms 1.3 MPa
100 ms 1.1 MPa
Normalized Firing rate
g
Spatial dispersion of activated cells (mm)
ns
*
****
0.5 MHz
2.25 MHz
15 MHz
h
Mean activated cells/ Stimulated area (mm²)
**
****
****
0.5 MHz
2.25 MHz
15 MHz
i
Moving US stimulus
15 MHz
+0.4 mm
+0.8 mm
200 ms 1.1 MPa
Normalized Firing rate
j
200 ms
1.1 MPa
Response displacement (mm)
****
**
US displacement (mm)

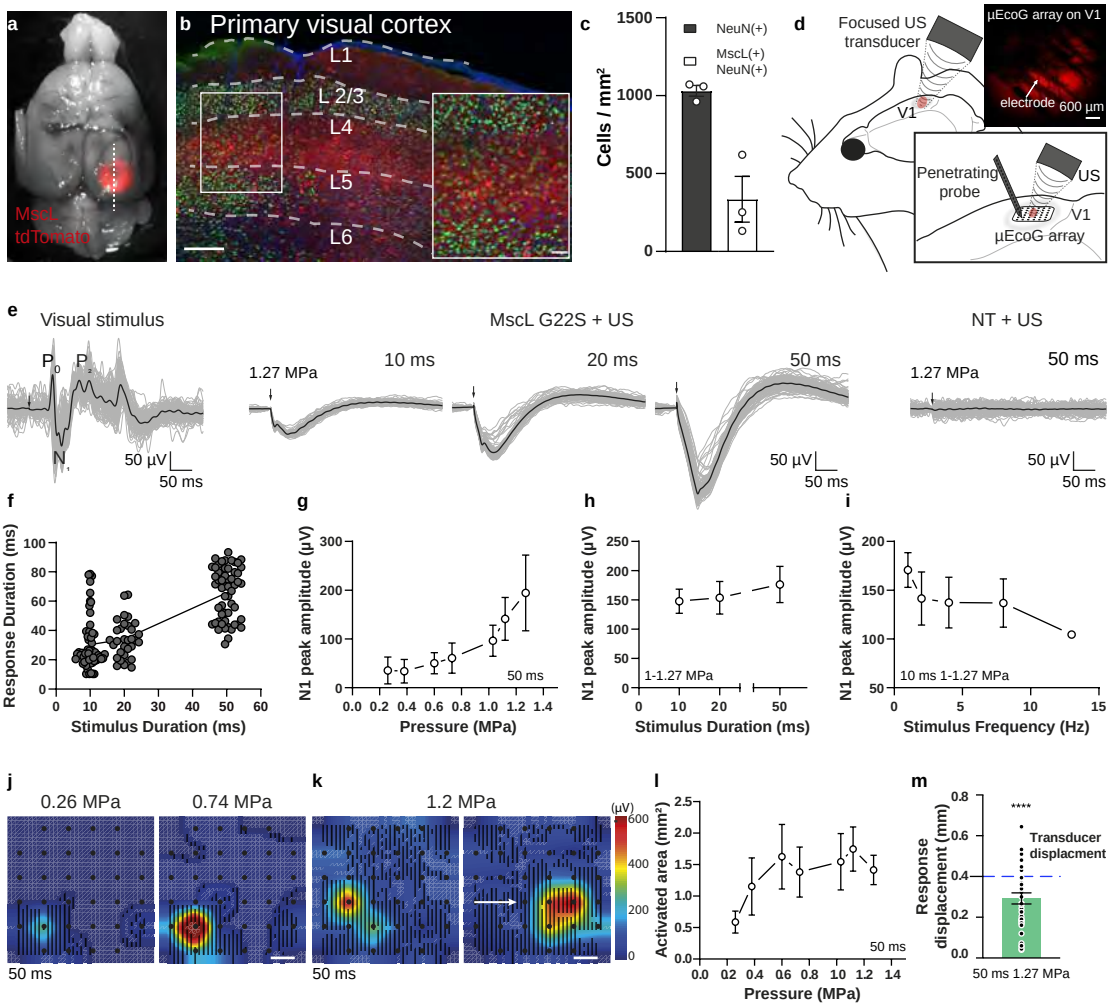
a
MscL
tdTomato
b
Primary visual cortex
L1
L 2/3
L4
L5
L6
c
Cells / mm²
1500
1000
500
0
NeuN(+)
MscL(+)
NeuN(+)
d
Focused US
transducer
V1
μEcoG array on V1
electrode
600 μm
Penetrating
probe
US
V1
μEcoG array
e
Visual stimulus
MscL G22S + US
NT + US
P1
P2
N1
50 μV
50 ms
1.27 MPa
10 ms
20 ms
50 ms
50 μV
50 ms
1.27 MPa
50 ms
50 μV
50 ms
f
Response Duration (ms)
Stimulus Duration (ms)
g
N1 peak amplitude (μV)
50 ms
Pressure (MPa)
h
N1 peak amplitude (μV)
1-1.27 MPa
Stimulus Duration (ms)
i
N1 peak amplitude (μV)
10 ms 1-1.27 MPa
Stimulus Frequency (Hz)
j
0.26 MPa
0.74 MPa
50 ms
k
1.2 MPa
(μV)
600
400
200
0
50 ms
l
Activated area (mm²)
50 ms
Pressure (MPa)
m
Response displacement (mm)
****
Transducer displacment
50 ms 1.27 MPa

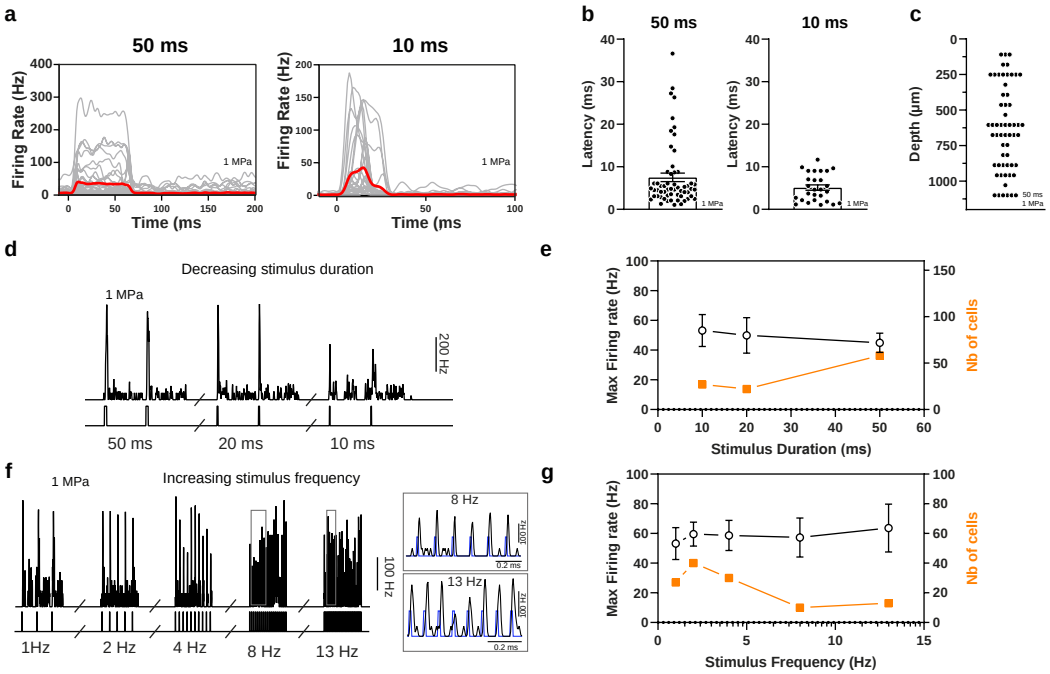
a
50 ms
10 ms
Firing Rate (Hz)
Time (ms
1 MPa
b
50 ms
10 ms
Latency (ms)
c
Depth (µm)
d
Decreasing stimulus duration
1 MPa
200 Hz
50 ms
20 ms
10 ms
e
Max Firing rate (Hz)
Nb of cells
Stimulus Duration (ms)
f
1 MPa
Increasing stimulus frequency
8 Hz
13 Hz
100 Hz
1Hz
2 Hz
4 Hz
8 Hz
13 Hz
g
Max Firing rate (Hz)
Nb of cells
Stimulus Frequency (Hz)

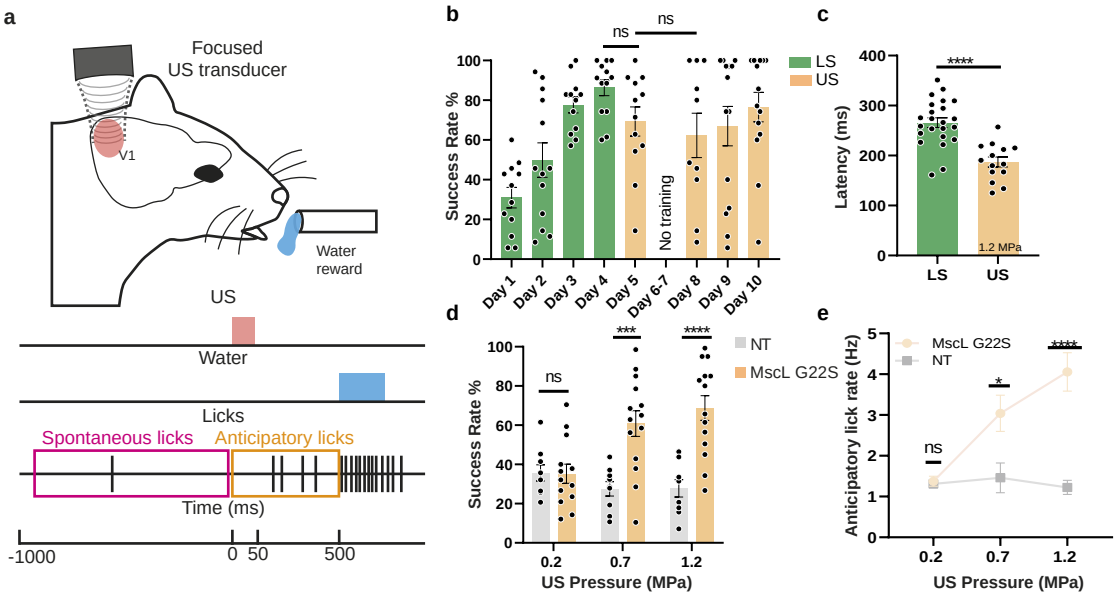
a
Focused
US transducer
V1
Water
reward
US
Water
Licks
Spontaneous licks
Anticipatory licks
Time (ms)
-1000
0
50
500
b
ns
ns
Success Rate %
No training
LS
US
Day 1
Day 2
Day 3
Day 4
Day 5
Day 6-7
Day 8
Day 9
Day 10
c
****
Latency (ms)
1.2 MPa
LS
US
d
ns
***
****
NT
MscL G22S
Success Rate %
US Pressure (MPa)
e
MscL G22S
NT
ns
*
****
Anticipatory lick rate (Hz)
US Pressure (MPa)

Extended data figures:

Fig. E1 Retinal expression of MscL. (a) Whole-mount retina expressing MscL WT (red) and labeled with the RGC-specific anti-RBPMS antibody (green), with DAPI staining of the nucleus (white). Yellow boxes represent the 8 zones selected for the counting of MscL- and RBPMS-positive cells. (b) Optical section of a confocal stack showing MscL expression limited to the ganglion cell layer. The scale bars represent 1 mm in (a), 50 µm in (b). Similar results have been obtained for N=10 retinas (5 expressing MscL WT and 5 expressing MscL G22s).

Fig.E2 Retinal sonogenetic response characteristics for US stimuli of different frequencies. (a) Mean distribution of the different RGC cell types (ON, OFF, ON-OFF) among short (SL) and long latency (LL) responses in retinas (*n*=9) expressing MscL (WT and G22s form) following a 15 MHz US stimulus (SD: 21.6, 28.0, 21.8 % for SL, 34.7, 19.4, 30.3 % for LL cells, for ON, ON-OFF and OFF cells respectively). (b) Mean numbers of RGCs responding to a 15 MHz stimulus of increasing acoustic pressure for MscL WT (*n*=3), MscL G22s (*n*=5) and NT (*n*=4) retinas (0.39 MPa: * *p*=0.0163; 0.54 MPa: ns *p*=0.1480, * *p*=0.0168; 0.74 MPa: ns *p*=0.1334, * *p*=0.0312; 0.96 MPa: * *p*=0.0462, * *p*=0.0279; 1.15 MPa: ns *p*=0.1617, * *p*=0.0145; 1.27 MPa: ns *p*=0.1580, * *p*=0.0144; unpaired two-tailed *t* test between MscL WT and NT in gray and MscL-G22s and NT in blue). (c) Scatter plots and geometric means of RGC latencies in response to a 15 MHz US stimulus for MscL (*n*=300 cells SD: 48.8), Blockers+MscL (*n*=57 cells, SD: 68.0), P23H+MscL (*n*=97 cells, SD: 37.5), and NT (*n*=41 cells, SD: 27.4) retinas (****, p=$7.3*10^{-8}$ for MscL and Blockers MscL vs NT and *p*<$.1*10^{-15}$ for P23H MscL vs NT, unpaired two-tailed *t*-test on log-transformed values). (d) Cumulative frequency distribution of RGC latencies for MscL, Blockers+MscL, P23H+MscL, and NT retinas. (e) Mean percentage of cells responding to US stimuli (normalized against the maximum number of responsive cells in the experiment) of increasing acoustic pressure for 0.5 MHz (ns *p*=0.1661;* *p*=0.0292; * *p*=0.0260; ns *p*=0.8628; ns *p*=0.1316; ns *p*=0.7731; unpaired *t* test,), 2.25 MHz (ns *p*=0.1474; ns *p*=0.0522; * *p*=0.0140; *** *p*=0.0005; **** *p*<0.00002; ns *p*=0.5000; unpaired *t* test) and 15 MHz US (* *p*=0.0382;** *p*=0.0065; * *p*=0.0218; ns *p*=0.8628; ns *p*=0.5859; ns *p*=0.4223; unpaired *t* test) US. The lower *x* axis represents the corresponding acoustic intensity (Ispta). (f) Mean response latencies of SL cells for 0.5 and 2.25 MHz (*n*=9 and 8 retinas). Data are presented as mean values +/- SEM.

Fig. E3 Experimentally measured US pressure fields. US pressure fds near the focus for 0.5, 2.25 and 15 MHz focused transducers, measured in water. Color-coded pressure maps in the *xy* and *xz* planes, for 0.5, 2.25 and 15 MHz.

Fig. E4 Simulated acoustic fields and temperature increases. (a) Comparison between a water tank measurement at the focus with a calibrated hydrophone (black) obtained with the 2.25 MHz transducer and reaching -1.11 MPa peak negative pressure, and a simulated waveform at the focus (blue) reaching the same negative pressure. The two waveforms match very well (0.42% error) ensuring a good match between our simulation setup and physical parameters. (b) Power spectral density of the measured (black) and simulated (blue) waveforms, showing that simulations can be used to estimate the importance of non-linear propagation. A second harmonic 20 dB below the fundamental indicates a factor of 100 in terms of energy, meaning that absorption can be calculated in a linear approximation. (c-f) Thermal simulations are performed in a two-fold process corresponding to a worst-case scenario (see methods): propagation in a water medium, and thermal absorption in a brain-mimicking medium. (h) 3D temperature map at the end of a 200 ms stimulation (at 15 MHz and 1.27 MPa). (d) Temperature rise at the focus for a 15 MHz 200 ms stimulation with the 7 pressures used in Fig. 1I (0.26, 0.39, 0.54, 0.74, 0.96, 1.15, 1.27 MPa). A zoom on the increasing curve reveals the fluctuations due to the 1 kHz on-off cycles. (e) Temperature rise at the focus for a 15 MHz 50 ms stimulation with the same 7 pressures. (f) Temperature rise at the focus for 15 MHz 10ms stimulations (1 kHz modulation) at a repetition rate of 8 Hz and 13 Hz (used in figure 3o), for focus pressures of 0.96 MPa and 0.54 MPa.

Fig. E5 In vivo response displacement to US stimulation. (a) Relative displacement of the activation center to the previous position following movement of the US transducer by 0.4 mm in the x and y direction (*n*=37 positions on 6 animals). Data are presented as mean values +/- SEM.

Fig. E6: MscL G22S expression with the US and light-associative training in mice. (a) Confocal stack projection of a sagittal brain slice expressing MscL G22s-tdTomato (red) and labeled with DAPI (blue). Similar results have been obtained on N=3 animals. (b) Head-fixed and water-restricted mice were trained for four days to respond to a full-field stimulation of one eye (200 and 50 ms) that preceded a water reward. Mice responded by licking before (anticipation — successful trial) or after the delivery of water (failure). The mean success rate increased progressively and mice learned the task (upon 50 ms and 200 ms light stimulation) after four days of training (ns p=0.9387, two-tailed unpaired t test, Mean: 27.9, 45.4, 77.1, 88.8, SD: 17.4, 24.8, 23.6, 10.4% for 200ms, Mean: 30.7, 54.2, 75.9, 88.5, SD: 22.2, 31.0, 17.5, 12.8% for 50ms). (c) Mean rates of successful trials in non-transfected (NT) mice for 4 days of training with light stimulation (50 ms, LS green) and for 4 days of US stimulation (US orange) (Between Day 4 LS and Day 5 US: 50 ms 1.2 MPa, ****, p=0.0000047, two-tailed unpaired t test. Between Day 5 US and Day 8 US: 50 ms 1.2 MPa, ns, p=0.1850. Mean: 30.5, 60.3, 73.6, 91.7, 38.1, 23.5, 14.3, 34.0, SD: 28.2, 31.6, 22.1, 10.3, 18.5, 25.5, 21.1, 24.4 %). (d) Pearson correlation scatter plot for time to first lick after either light (LS) or US stimulation. (e) Identification and exclusion of outlier sessions (in red) based on the ROUT method, (Q = 1%) for the session spontaneous lick rate measured on a 1s time window prior to all trials of the session e Q_1= 0.9 Hz, Median = 1.7 Hz, Q_3= 2.8 Hz, Mean= 2.3 Hz, SD= 2.3 Hz. Data are presented as mean values +/- SEM.


a
MscL-Tdt
RBPMS
DAPI
b
GCL
IPL
INL
OPL
ONL
MscL-Tdt
DAPI

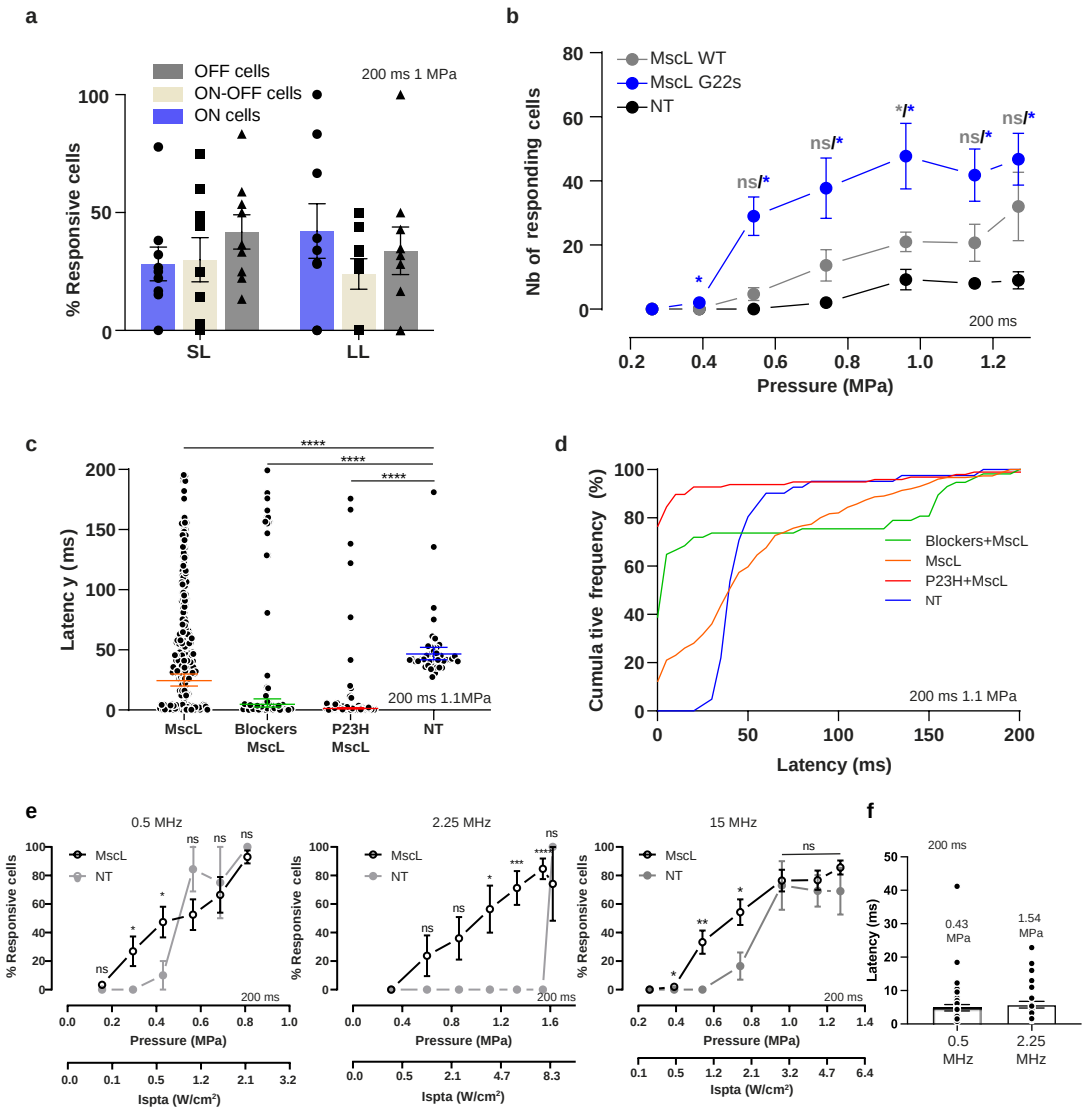
a
OFF cells
ON-OFF cells
ON cells
200 ms 1 MPa
% Responsive cells
SL
LL
b
MscL WT
MscL G22s
NT
Nb of responding cells
Pressure (MPa)
200 ms
c
Latenc y (ms)
MscL
Blockers MscL
P23H MscL
NT
200 ms 1.1MPa
d
Cumula tive frequency (%)
Blockers+MscL
MscL
P23H+MscL
NT
200 ms 1.1 MPa
Latency (ms)
e
0.5 MHz
2.25 MHz
15 MHz
% Responsive cells
Pressure (MPa)
Ispta (W/cm²)
f
Latency (ms)
0.43 MPa
1.54 MPa
0.5 MHz
2.25 MHz

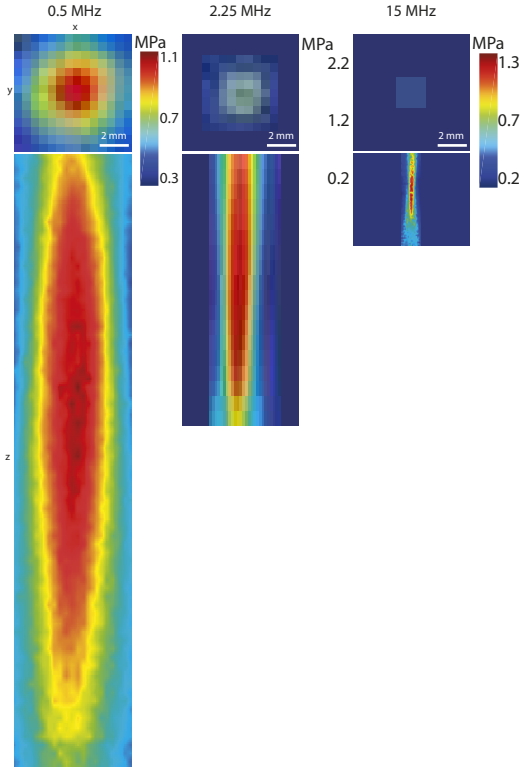
0.5 MHz
2.25 MHz
15 MHz
x
y
z
MPa
1.1
0.7
0.3
2 mm
MPa
2.2
1.2
0.2
2 mm
MPa
1.3
0.7
0.2
2 mm

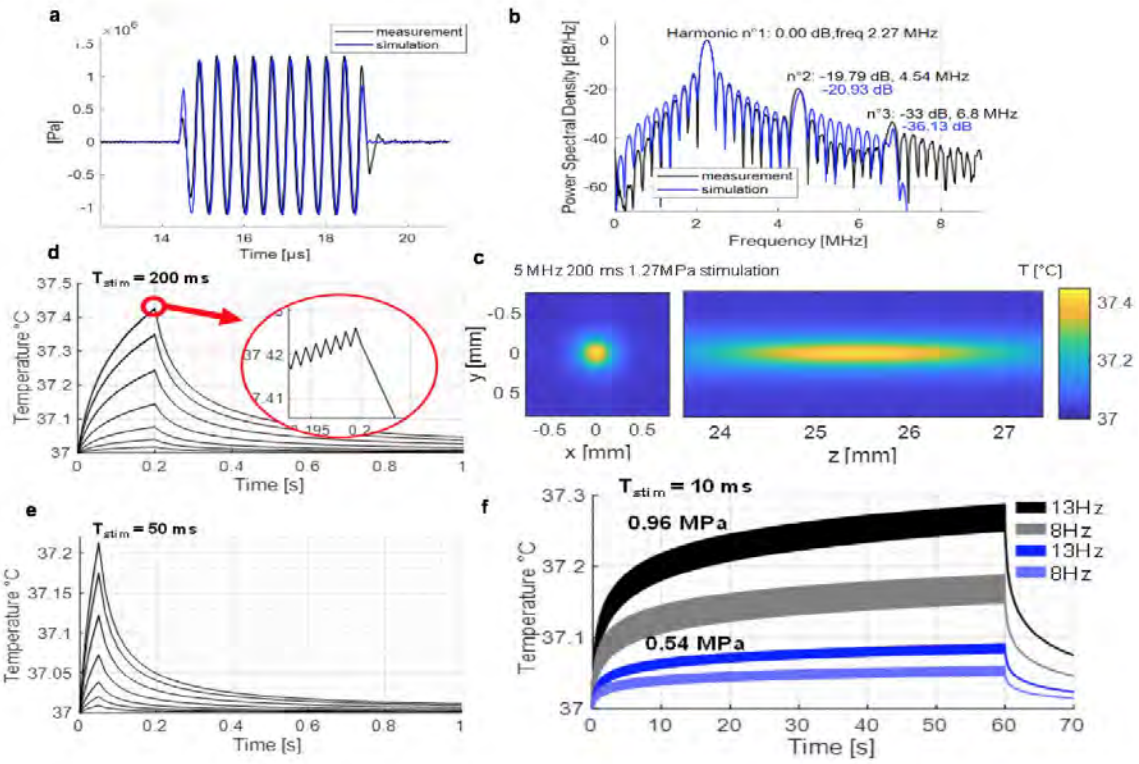
a
measurement
simulation
[Pa]
Time [µs]
b
Harmonic n°1: 0.00 dB,freq 2.27 MHz
n°2: -19.79 dB, 4.54 MHz
-20.93 dB
n°3: -33 dB, 6.8 MHz
-36.13 dB
Power Spectral Density [dB/Hz]
Frequency [MHz]
c
5 MHz 200 ms 1.27MPa stimulation
T [°C]
y [mm]
x [mm]
z [mm]
d
T_stim = 200 ms
Temperature °C
Time [s]
e
T_stim = 50 ms
Temperature °C
Time [s]
f
T_stim = 10 ms
0.96 MPa
0.54 MPa
13Hz
8Hz
13Hz
8Hz
Temperature °C
Time [s]

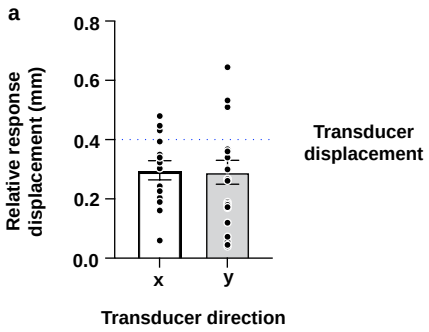
a
0.8
0.6
0.4
0.2
0.0
Relative response displacement (mm)
Transducer displacement
x
y
Transducer direction

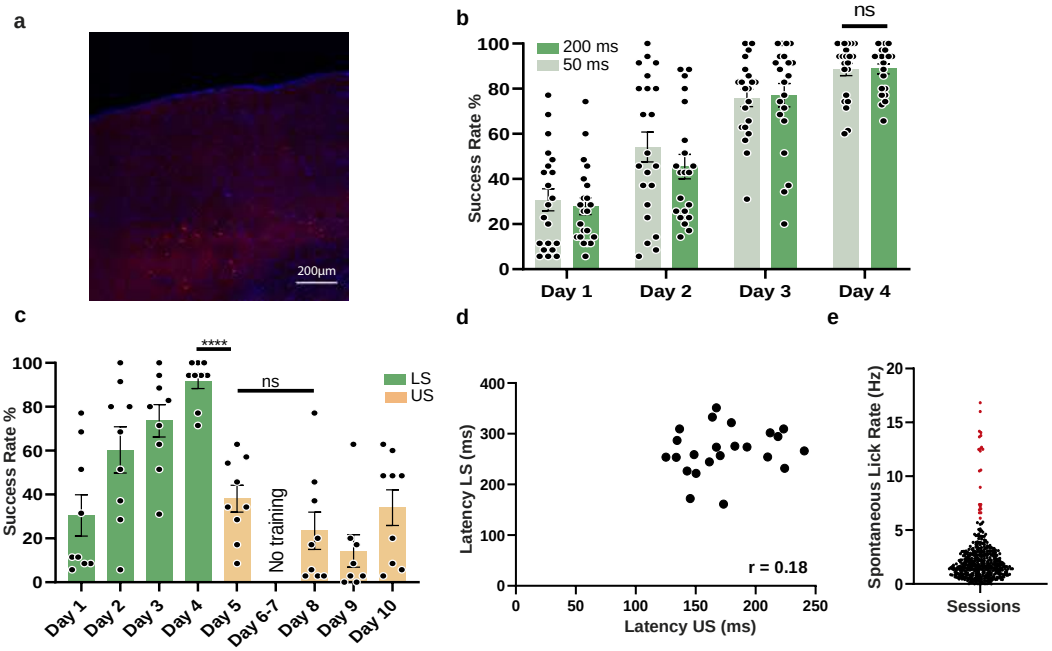
a
200µm
b
ns
200 ms
50 ms
Success Rate %
Day 1
Day 2
Day 3
Day 4
c
****
ns
LS
US
No training
Success Rate %
Day 1
Day 2
Day 3
Day 4
Day 5
Day 6-7
Day 8
Day 9
Day 10
d
Latency LS (ms)
r = 0.18
Latency US (ms)
e
Spontaneous Lick Rate (Hz)
Sessions